The Annals of Applied Probability
2026, Vol. 36, No. 4, 3601–3634
https://doi.org/10.1214/26-AAP2314

NUMERICAL SIMULATION OF GENERALIZED HERMITE PROCESSES

BY ANTOINE AYACHE[1,a], JULIEN HAMONIER[2,b] AND LAURENT LOOSVELDT[3,c]

[1]*Univ. Lille, CNRS, UMR 8524—Laboratoire Paul Painlevé,* [a]*antoine.ayache@univ-lille.fr*
[2]*Univ. Lille, CHU Lille, ULR 2694—METRICS: Évaluation des technologies de santé et des pratiques médicales,* [b]*julien.hamonier@univ-lille.fr*
[3]*Université de Liège, Département de Mathématique,* [c]*l.loosveldt@uliege.be*

Hermite processes are paradigmatic examples of stochastic processes which can belong to any Wiener chaos of an arbitrary order; the well-known fractional Brownian motion belonging to the Gaussian first order Wiener chaos and the Rosenblatt process belonging to the non-Gaussian second order Wiener chaos are two particular cases of them. Except for these two particular cases no simulation method for sample paths of Hermite processes is available so far. The goal of our article is to introduce a new method which potentially allows to simulate sample paths of any Hermite process and even those of any generalized Hermite process.

Our starting point is the representation for the latter process as random wavelet-type series, obtained in our very recent paper (*Constr. Approx.* **61** (2025) 535–601). We construct from it a "concrete" sequence of piecewise linear continuous random functions which almost surely approximate sample paths of this process for the uniform norm on any compact interval, and we provide an almost sure estimate of the approximation error. Then, for the Rosenblatt process and more importantly for the third order Hermite process as well as its generalized version, we propose algorithms allowing to implement this sequence and we illustrate them by several simulations. Python routines implementing these synthesis procedures are available upon request.

1. Introduction and motivation. For many years, there has been growing interest in modelling many real-life situations using fractional stochastic processes. Among other things, these families of parametrized processes offer a natural framework for simulating phenomena with short- or long-range dependence properties, as well as self-similarity. We refer, for example, to the monographs [20, 22] for a comprehensive view on both properties. A standard strategy consists in using the famous fractional Brownian motion [29]. This process has been for instance used for simulations in astronomy [37], biology [21], climatology [25], image processing [30], internet traffic modelling [35] and physics [31]. The fractional Brownian motion of Hurst parameter $H \in (0,1)$ on a probability space $(\Omega, \mathcal{F}, \mathbb{P})$ is known to be the unique centred Gaussian process $\{B_t^H\}_{t\geq 0}$ with covariance function given, for all, $s, t \geq 0$, by

$$\mathbb{E}\big[B_t^H B_s^H\big] = \frac{1}{2}\big(|t|^{2H} + |s|^{2H} - |t-s|^{2H}\big). \tag{1}$$

To numerically simulate a fractional Brownian motion, one can use a wavelet-based synthesis, which relies on its wavelet-type random series representation due to Meyer, Sellan and Taqqu [32]. We refer to the papers [2, 15] for details and practical features about the implementation of such an algorithm. Note that, in this Gaussian case, exact simulation methods are available, meaning that the data are drawn exactly from the distribution defined by the process, without incurring approximation errors. We refer, for instance, to the book [41] for

Received November 2024; revised February 2026.
MSC2020 subject classifications. Primary 60G22, 60G18, 42C40; secondary 41A58.
Key words and phrases. High order Wiener chaos, self-similar processes, Hermite processes, FARIMA sequences, wavelet-type expansions, simulations.

an overview of various simulation methods, including the Cholesky decomposition. For detailed studies and extensions of the now widely used circulant matrix method, we refer to [14, 18, 27, 54] and the references therein. The core idea behind this approach is that a Gaussian process is uniquely characterized by its mean and covariance functions. However, this fundamental property does not hold in the non-Gaussian setting considered in the present paper. Indeed, in many situations, the Gaussianity of the fractional Brownian motion is a too strong assumption to model a phenomenon of interest. Such a case arises, for instance, in mathematical finance [24, 47], hydrology [48] or internet traffic modelling [52]. To drop the Gaussian assumption, one can use the affiliation of fractional Brownian motion in the family of Hermite processes.

For $d \geq 1$ and $H \in (1/2, 1)$, the Hermite process of order d and Hurst parameter H is defined, at any time $t \in \mathbb{R}_+$, by the multiple Wiener integral

$$\sqrt{\frac{H(2H-1)}{d!\beta(\frac{1}{2}-\frac{1-H}{d},\frac{2-2H}{d})^d}}\int_{\mathbb{R}^d}'\left(\int_0^t\prod_{\ell=1}^d(s-x_\ell)_+^{\frac{H-1}{d}-\frac{1}{2}}\,ds\right)dB(x_1)\cdots dB(x_d), \tag{2}$$

where $\{B(x)\}_{x\in\mathbb{R}}$ is a usual Brownian motion, β denotes the classical Euler's Beta function[1] and we use the convention that, for all $(x,\alpha)\in\mathbb{R}^2$,

$$x_+^\alpha := \begin{cases} x^\alpha & \text{if } x>0,\\ 0 & \text{otherwise.}\end{cases}$$

Observe that the symbol $\int_{\mathbb{R}^d}'$ in (2) denotes integration over $\mathbb{R}^d$ with diagonals $\{x_\ell = x_{\ell'}\}$, $\ell \neq \ell'$, excluded. It is the paradigmatic example of a stochastic process in the Wiener chaos of order d. When $d=1$, it reduces to the fractional Brownian motion, which is the only Gaussian process in this family. The Hermite process of any order is H-self-similar, has stationary increments, exhibits long-range dependence and has the same covariance function (1) as the fractional Brownian motion. In particular, its sample paths are almost surely, on each compact interval and for every $\delta \in (0, H)$, Hölder continuous functions of order δ.

The Hermite process of order 2 is also known as the Rosenblatt process. In [1], the authors propose two practical methods for simulating its sample paths. They are based on its random wavelet-type series representation introduced in [38]. For the first method, the authors obtain a uniform convergence result [1], eq 2.5. Whereas for the second method, they formulate a conjecture concerning the uniform convergence on any compact set of their representation [1], eq 2.10. Also we mention that in [49] the authors propose an algorithm based on a Donsker-type theorem to numerically approximate the Rosenblatt process by perturbed random walks. Nevertheless, the rate of convergence of this approximation procedure is not provided by them.

In [38], the author raises the question of whether the wavelet-type expansion he obtains for the Rosenblatt process can be extended to any Hermite process. This problem remained open up to our very recent work [5]. In the latter paper, we even consider a larger family of processes which contains the Hermite ones (see Definition 2.1 below). We provide a wavelet-type expansion for any process in this family which, among other things, offers the advantage to clearly separate the low and high frequency parts of the process. Moreover, we obtain an explicit estimate for the rate of convergence of the low frequency part towards its corresponding process.

Despite the growing interest for Hermite processes in the literature, up to now, there is no method to numerically simulate sample paths of such a process, as soon as the order $d \geq 3$; the

[1] for all $x, y > 0$, $\beta(x,y) = \int_0^1 t^{x-1}(1-t)^{y-1}\,dt$.

latter fact is mentioned on page 43 of the very recent book [50]. The aim of the current paper is to make a breakthrough in this area in order to overcome the serious drawback due to the lack of simulation methods. Our starting point is the representation of any arbitrary generalized Hermite process as random wavelet-type series, obtained in our very recent paper [5]. The main lines of the latter article can somehow be divided into two distinct parts, following the classical scheme of wavelet-based approximation methods:

- First, we derived an expression for the low-frequency component of the process in terms of a random series based on Gaussian FARIMA processes and well localized fractional scaling functions. Then we ensured that this random series converges almost surely and uniformly on compact intervals. That is, Theorem 2.8 and Section 3 in [5].
- Second, we decomposed the corresponding high-frequency component into several wavelet-based random series, from which we managed to estimate the rate of convergence of the low-frequency part towards the target process. That is, Theorem 2.12 and Section 4 in [5].

In particular, in [5], we do not seek to truncate and simplify anymore the random series representing the low-frequency component for approximation purposes. This stands in sharp contrast to the current paper. Indeed, the results from [5], which are summarized in Theorem 2.7 here below, still cannot be directly exploited for the numerical simulation of Hermite processes. In fact, since the "low-frequency" component (see (15) in Theorem 2.7 below) is an infinite sum of functions weighted by sums of products of FARIMAs, its numerical implementation would require the simulation of infinitely many FARIMAs and rather complicated functions—which is, of course, not feasible in practice. A main goal of the current paper is to appropriately truncate and modify this random series "low-frequency", so that one obtains from it a "concrete" piecewise linear continuous random function which almost surely approximates sample paths of the corresponding (generalized) Hermite process for the uniform norm on any compact interval. Moreover, our approach has the advantage of providing an explicit estimate for the rate of convergence. It is worth highlighting that this estimate matches the one we previously obtained in [5] for the rate of convergence of the low-frequency component towards the corresponding (generalized) Hermite process. From this perspective, our strategy does not entail any loss of accuracy. In the last section of the current paper, for the Rosenblatt process and more importantly for the third order Hermite process, as well as its generalized version, we propose algorithms allowing to implement this sequence of "approximation processes" and we illustrate them by several simulations.

We believe that our work could be of potential interest for applications for which (generalized) Hermite processes are underlying models. Among other things, it can be used to test numerical efficiency of various statistical estimators for the Hurst parameter of Hermite processes, based, for instance, on quadratic variations [6, 11, 51], (approached) maximum (log-)likelihood [8, 17, 42, 53], log-periodogram [34] or wavelet variations [9, 13, 28].

The rest of the paper is organized as follows. In Section 2, we first precisely define the class of generalized Hermite processes as well as their wavelet-type random series representation. Then we state our two main results which are issued from the latter representation. Section 3 is devoted to their proofs which are, on one hand, to a certain extent, inspired by some ideas from [5] and, on another hand, contain significant novelties with respect to [5] as, for instance Lemmata 3.4 and 3.6. In Section 4, we provide algorithms allowing to numerically simulate the Rosenblatt process and more importantly the Hermite process of order 3, as well as the generalized Hermite process of order 3. Then we test these algorithms through several simulations. Finally, Section 5 is devoted to numerical experiments devoted to the validation of our procedure.

2. Background and statement of the main results. The family of processes we are interested in, called generalized Hermite processes, was introduced in [7]. These processes are self-similar and have stationary increments. They include Rosenblatt and any other Hermite process [40], Chapter 4.

DEFINITION 2.1. The generalized Hermite process of any arbitrary order $d \geq 2$, denoted by $\{X_{\mathbf{h}}^{(d)}(t)\}_{t\in\mathbb{R}_+}$, depends on a vector-valued Hurst parameter $\mathbf{h} := (h_1, \ldots, h_d)$ whose coordinates satisfy

$$h_1, \ldots, h_d \in (1/2, 1) \quad \text{and} \quad \sum_{\ell=1}^{d} h_\ell > d - \frac{1}{2}. \tag{3}$$

This process belongs to the non-Gaussian dth Wiener chaos, since it is defined, for each $t \in \mathbb{R}_+$, through the multiple Wiener integral:

$$X_{\mathbf{h}}^{(d)}(t) := \int_{\mathbb{R}^d}' K_{\mathbf{h}}^{(d)}(t, x_1, \ldots, x_d)\, dB(x_1) \cdots dB(x_d), \tag{4}$$

where the deterministic kernel function $K_{\mathbf{h}}^{(d)}$ is given, for every $(t, x_1, \ldots, x_d) \in \mathbb{R}_+ \times \mathbb{R}^d$, by

$$K_{\mathbf{h}}^{(d)}(t, x_1, \ldots, x_d) := \frac{1}{\prod_{\ell=1}^{d} \Gamma(h_\ell - 1/2)} \int_0^t \prod_{j=1}^{d} (s - x_\ell)_+^{h_\ell - 3/2}\, ds. \tag{5}$$

REMARK 2.2. As mentioned in [7], Theorem 3.5., the process $\{X_{\mathbf{h}}^{(d)}(t)\}_{t\in\mathbb{R}_+}$ has stationary increments and is self-similar with self-similarity index $H \in (1/2, 1)$ given by

$$H := \left(\sum_{\ell=1}^{d} h_\ell\right) - d + 1. \tag{6}$$

One can derive from these two nice properties that, for any indices $s, t \in \mathbb{R}_+$ and exponent $p > 0$,

$$\mathbb{E}\big[|X_{\mathbf{h}}^{(d)}(t) - X_{\mathbf{h}}^{(d)}(s)|^p\big] = |t - s|^{Hp}\mathbb{E}\big[|X_{\mathbf{h}}^{(d)}(1)|^p\big]. \tag{7}$$

Moreover, one knows from the hypercontractivity property for multiple Wiener integrals (see, e.g., [36], Theorem 2.7.2) that, for all $p > 0$, one has $\mathbb{E}[|X_{\mathbf{h}}^{(d)}(1)|^p] < \infty$. Thus, it follows from (7) and Kolmogorov continuity theorem that there exists a modification of $\{X_{\mathbf{h}}^{(d)}(t)\}_{t\in\mathbb{R}_+}$ and Ω_1, an event of probability 1, such that, on Ω_1, sample paths of this modification are locally (i.e., on each compact interval) γ-Hölder continuous functions, for any $\gamma \in (0, H)$. All along this paper, we identify $\{X_{\mathbf{h}}^{(d)}(t)\}_{t\in\mathbb{R}_+}$ with this modification. Thus, one can write that, for each fixed $T > 0$ and $\gamma \in (0, H)$, there is a positive finite random variable $C_{T,\gamma}$ such that, almost surely, for every $s, t \in [0, T]$, the following inequality holds:

$$|X_{\mathbf{h}}^{(d)}(t) - X_{\mathbf{h}}^{(d)}(s)| \leq C_{T,\gamma}|s - t|^\gamma. \tag{8}$$

REMARK 2.3. Observe that when all the coordinates $h_1, \ldots, h_d$ of the vector-valued parameter $\mathbf{h}$ are equal to $1 + \frac{H-1}{d}$, then the process $\{X_{\mathbf{h}}^{(d)}(t)\}_{t\in\mathbb{R}_+}$ reduces to the usual Hermite process of Hurst parameter H and order d, up to a renormalisation. The constant $\sqrt{\frac{H(2H-1)}{d!\beta(\frac{1}{2}-\frac{1-H}{d}, \frac{2-2H}{d})^d}}$ used in (2) is chosen such that the process at time 1 has unit variance. On the other side, the constant $\frac{1}{\prod_{\ell=1}^{d}\Gamma(h_\ell - 1/2)}$ used in (5) is more practicable for computation in the general context of Definition 2.1.

In order to state and motivate the main results of the present article, first we need to recall some notation and fundamental results from our previous paper [5]. The two real-valued functions ϕ and ψ are respectively a univariate scaling function and a mother wavelet associated with a Meyer orthonormal wavelet basis of $L^2(\mathbb{R})$. Recall that ϕ and ψ belong to the Schwartz class $\mathcal{S}(\mathbb{R})$ of infinitely differentiable functions whose derivatives of any order rapidly decay at infinity. Moreover, the Fourier transforms $\widehat{\phi}$ and $\widehat{\psi}$ are infinitely differentiable compactly supported functions satisfying

$$\operatorname{supp}\widehat{\phi} \subseteq \left[-\frac{4\pi}{3}, \frac{4\pi}{3}\right] \quad \text{and} \quad \operatorname{supp}\widehat{\psi} \subseteq \left[-\frac{8\pi}{3}, \frac{8\pi}{3}\right] \setminus \left(-\frac{2\pi}{3}, \frac{2\pi}{3}\right).$$

The wavelet-type expansion of generalized Hermite process relies on the fractional primitives ψ_h of the mother wavelet ψ defined in Definition 2.4 below. We refer to the book [43] for a detailed presentation of the notions of fractional primitive and fractional derivative and related topic, also we refer to [32], Section 4.

DEFINITION 2.4. For all $h \in [1/2, +\infty)$ (resp. $h \in (-\infty, 1/2)$), the fractional primitive of ψ of order $h - 1/2$ (resp. the fractional derivative of ψ of order $1/2 - h$) is the function $\psi_h \in \mathcal{S}(\mathbb{R})$ defined through its Fourier transform by:

$$\widehat{\psi_h}(0) := 0 \text{ and, for all } \xi \neq 0 \quad \widehat{\psi_h}(\xi) := (i\xi)^{1/2-h}\widehat{\psi}(\xi).$$

Note that, since the compactly supported Fourier transform $\widehat{\psi}$ vanishes in a neighbourhood of 0, fractional primitives and derivatives of a univariate Meyer mother wavelet ψ belong to the Schwartz class $\mathcal{S}(\mathbb{R})$. At the opposite, since $\widehat{\phi}(0) = 1 \neq 0$, fractional primitives and derivatives of a univariate Meyer scaling function ϕ fail to be smooth well-localized functions. In order to overcome this serious difficulty, a clever idea of [32] was to "replace" fractional primitive or derivative of ϕ by the so-called fractional scaling function $\Phi_\Delta^{(\delta)}$, which belongs to $\mathcal{S}(\mathbb{R})$ and which was defined in [32] as follows:

DEFINITION 2.5. The *fractional scaling function* of order $\delta \in (-\infty, +\infty)$ of a univariate Meyer scaling function ϕ is the function $\Phi_\Delta^{(\delta)} \in \mathcal{S}(\mathbb{R})$ defined through its Fourier transform by:

$$\widehat{\Phi}_\Delta^{(\delta)}(\xi) := \left(\frac{1 - e^{-i\xi}}{i\xi}\right)^\delta \widehat{\phi}(\xi) \quad \forall \xi \neq 0 \text{ and } \widehat{\Phi}_\Delta^{(\delta)}(0) := 1.$$

Notice that, similar to $\widehat{\phi}$, the function $\widehat{\Phi}_\Delta^{(\delta)}$ has a compact support satisfying

$$\operatorname{supp}\widehat{\Phi}_\Delta^{(\delta)} \subseteq \left[-\frac{4\pi}{3}, \frac{4\pi}{3}\right]. \tag{9}$$

One can check, by using elementary properties of the Fourier transform on the space $\mathcal{S}(\mathbb{R})$ (see, e.g., the seminal book [45]), that $\Phi_\Delta^{(\delta)}$ and ψ_h are well-defined functions belonging to $\mathcal{S}(\mathbb{R})$, which means that they are infinitely differentiable functions satisfying, for all $m \in \mathbb{N}_0$ and $L > 0$,

$$\sup_{x\in\mathbb{R}}\left\{(3 + |x|)^L\left(\left|\frac{d^m}{dx^m}\Phi_\Delta^{(\delta)}(x)\right| + \left|\frac{d^m}{dx^m}\psi_h(x)\right|\right)\right\} < +\infty. \tag{10}$$

Another fundamental ingredient of the wavelet-type expansion of generalized Hermite process is the so-called Gaussian FARIMA (autoregressive fractionally integrated moving average) sequence defined as follows.

DEFINITION 2.6. Generally speaking, if $\{X_k\}_{k\in\mathbb{Z}}$ is a time series, we consider the backshift operator $\mathfrak{B}$ defined, for each $k\in\mathbb{Z}$, as $\mathfrak{B}X_k = X_{k-1}$. Then, for any $\delta\in(-1/2,1/2)$, given a sequence $(Z_k)_{k\in\mathbb{Z}}$ of i.i.d. centred Gaussian random variables, the Gaussian FARIMA $(0,\delta,0)$ sequence $(Z_k^{(\delta)})_{k\in\mathbb{Z}}$ is defined, for each $k\in\mathbb{Z}$, as

$$Z_k^{(\delta)} := (I-\mathfrak{B})^{-\delta} Z_k = \sum_{p=0}^{+\infty} \gamma_p^{(\delta)} \mathfrak{B}^p Z_k = \sum_{p=0}^{+\infty} \gamma_p^{(\delta)} Z_{k-p},$$

where we have set

$$\gamma_0^{(\delta)} = 1 \text{ and, for all } p\in\mathbb{N},\quad \gamma_p^{(\delta)} := \frac{\delta\Gamma(p+\delta)}{\Gamma(p+1)\Gamma(\delta+1)}.$$

In the context of generalized Hermite process, we extended this definition to cover the case of chaotic random variables. Namely, we consider, for all $J\in\mathbb{Z}$, the sequence of dth Wiener chaos random variables

$$\left(\mu_{J,\mathbf{k}} := 2^{J\frac{d}{2}} \int_{\mathbb{R}^d}{}' \phi(2^J x_1 - k_1)\cdots\phi(2^J x_d - k_d)\, dB(x_1)\ldots dB(x_d)\right)_{\mathbf{k}\in\mathbb{Z}^d}$$

and set, for all $\mathbf{h}$ satisfying (3),

$$\sigma_{J,\mathbf{k}}^{(\mathbf{h})} := \sum_{\mathbf{p}\in\mathbb{N}_0^d} \left(\prod_{l=1}^{d} \gamma_{p_l}^{(h_l-1/2)}\right) \mu_{J,\mathbf{k}-\mathbf{p}}. \tag{11}$$

Also, we remarked that if we consider, for $J\in\mathbb{Z}$, the Gaussian FARIMA $(0,\delta,0)$ sequence $(Z_{J,\ell}^{(\delta)})_{\ell\in\mathbb{Z}}$ associated to the sequence of the i.i.d. standard Gaussian random variables

$$\left(g_{J,k}^{\phi} := 2^{J/2}\int_{\mathbb{R}} \phi(2^J x - k)\, dB(x)\right)_{k\in\mathbb{Z}},$$

then we get, the more explicit expression [5], Proposition 2.7, for all $\mathbf{k}\in\mathbb{Z}^d$,

$$\sigma_{J,\mathbf{k}}^{(\mathbf{h})} = \sum_{m=0}^{\lfloor d/2\rfloor} (-1)^m \sum_{P\in\mathcal{P}_m^{(d)}} \prod_{r=1}^{m} \mathbb{E}[Z_{J,k_{\ell_r}}^{(h_{\ell_r}-1/2)} Z_{J,k_{\ell_r'}}^{(h_{\ell_r'}-1/2)}] \prod_{s=m+1}^{d-m} Z_{J,k_{\ell_s''}}^{(h_{\ell_s''}-1/2)}, \tag{12}$$

where $\mathcal{P}_m^{(d)}$ is the finite set of all partitions of $\{1,\ldots,d\}$ with m (nonordered) pairs and $d-2m$ singletons and the indices ℓ_r, ℓ_r' and ℓ_s'' are such that

$$P = \{\{\ell_1,\ell_1'\},\ldots,\{\ell_m,\ell_m'\},\{\ell_{m+1}''\},\ldots,\{\ell_{d-m}''\}\}.$$

Finally, for all $\mathbf{j},\mathbf{k}\in\mathbb{Z}^d$, we set

$$\psi_{\mathbf{j},\mathbf{k}} := \bigotimes_{\ell=1}^{d} \psi_{j_\ell,k_\ell}, \tag{13}$$

where $\psi_{j_\ell,k_\ell}(\cdot) := 2^{j_\ell/2}\psi(2^{j_l}\cdot - k_\ell)$, and we consider the chaotic random variable

$$\varepsilon_{\mathbf{j},\mathbf{k}} := \int_{\mathbb{R}^d}{}' \psi_{\mathbf{j},\mathbf{k}}(x_1,\ldots,x_d)\, dB(x_1)\ldots dB(x_d). \tag{14}$$

Theorem 2.8 and Theorem 2.12 of [5] can then be summarized together as follows.

THEOREM 2.7. *The random series*

$$X^{(d)}_{\mathbf{h},J}(t) = 2^{-J(h_1+\cdots+h_d-d)} \sum_{\mathbf{k}\in\mathbb{Z}^d} \sigma^{(\mathbf{h})}_{J,\mathbf{k}} \int_0^t \prod_{\ell=1}^{d} \Phi_\Delta^{(h_\ell-1/2)}\big(2^J s - k_\ell\big)\, ds, \tag{15}$$

is almost surely, for each fixed $J \in \mathbb{N}$, uniformly convergent in t on every compact interval $I \subset \mathbb{R}_+$. Moreover, for any such I, there exists an almost surely finite random variable (depending on I) for which one has, almost surely, for all $J \in \mathbb{N}$,

$$\big\| X^{(d)}_{\mathbf{h}} - X^{(d)}_{\mathbf{h},J} \big\|_{I,\infty}$$

$$= \left\| \sum_{\substack{(\mathbf{j},\mathbf{k})\in(\mathbb{Z}^d)^2 \\ \max_{\ell\in[\![1,d]\!]} j_\ell \geq J}} 2^{j_1(1-h_1)+\cdots+j_d(1-h_d)} \varepsilon_{\mathbf{j},\mathbf{k}} \int_0^t \prod_{\ell=1}^{d} \psi_{h_\ell}\big(2^{j_\ell} s - k_\ell\big)\, ds \right\|_{I,\infty} \tag{16}$$

$$\leq C J^{\frac{d}{2}} 2^{-J(h_1+\cdots+h_d-d+1/2)}. \tag{17}$$

In view of Theorem 2.7, we call $\{X^{(d)}_{\mathbf{h},J}(t)\}_{t\in\mathbb{R}_+}$ the *approximation process at scale J*. Unfortunately, it has not yet a form which is well adapted to numerical simulations. In order to overcome this difficulty we need to replace it by the stochastic process $\{S^{(d)}_{\mathbf{h},J}(t)\}_{t\in\mathbb{R}_+}$, called the *simulation process at scale J*, which will be defined in the sequel. We aim at doing so without altering the estimate of the rate of convergence given in the second part of Theorem 2.7. On this purpose, we recall the following definition of some important sets.

DEFINITION 2.8 ([5], Definition 4.3). Let a be a fixed real number satisfying $1/2 < a < 1$. For all $(j,k) \in \mathbb{Z}_+ \times \mathbb{Z}$, let us denote by $B_{j,k}$ the compact interval

$$B_{j,k} := \big[k2^{-j} - 2^{-ja}, k2^{-j} + 2^{-ja}\big]. \tag{18}$$

For all $j \in \mathbb{N}$ and for all $t \in \mathbb{R}_+$, we consider the three disjoint subsets of $\mathbb{Z}$:

$$D^1_j(t) := \big\{k \in \mathbb{Z} : B_{j,k} \subseteq [0,t]\big\}, \tag{19}$$

$$D^2_j(t) := \big\{k \in \mathbb{Z} \setminus D^1_j(t) : B_{j,k} \cap [0,t] \neq \varnothing\big\}, \tag{20}$$

$$D^3_j(t) := \big\{k \in \mathbb{Z} : B_{j,k} \cap [0,t] = \varnothing\big\}. \tag{21}$$

These three sets, depending on t and a, form a partition of $\mathbb{Z}$:

$$\mathbb{Z} = \bigcup_{\ell=1}^{3} D^\ell_j(t).$$

The set $(D^1_j(t))^d$ is the Cartesian product of the set $D^1_j(t)$ d-times with itself. In [5], we somehow remarked that the estimate of the rate of convergence in (17) is mainly determined by the terms of the series in (16) whose indices $\mathbf{k}$ belong to some $(D^1_j(t))^d$ sets, with $j \geq J$ and $t \in I$. Therefore, the idea behind the definition of $S^{(d)}_{\mathbf{h},J}(t)$, with $J \in \mathbb{N}$ and $t \geq 0$, is to use an appropriate enlargement of the "diagonal set" of $(D^1_J(t))^d$.

DEFINITION 2.9. Let ε be a fixed positive real number. For all $J \in \mathbb{N}$ and for all $t \in \mathbb{R}_+$, we consider the three subsets

$$\mathcal{J}^1_J(t) := \Big\{\mathbf{k} \in \big(D^1_J(t)\big)^d : \max_{\ell,\ell'\in[\![1,d]\!]} |k_\ell - k_{\ell'}| \leq 2^{\varepsilon J}\Big\}, \tag{22}$$

$$\mathcal{J}^2_J(t) := \big\{\mathbf{k} \in \mathbb{Z}^d : \exists n \text{ such that } k_n \in D^2_J(t)\big\}, \tag{23}$$

$$\mathcal{J}^3_J(t) := \{\mathbf{k} \in \mathbb{Z}^d : \exists n \text{ such that } k_n \in D^3_J(t)\}. \tag{24}$$

The simulation process $\{S^{(d)}_{\mathbf{h},J}(t)\}_{t\in\mathbb{R}_+}$ is then defined as follows.

DEFINITION 2.10. For all $J \in \mathbb{N}$, the *simulation process at scale* J of the generalized Hermite process $\{X^{(d)}_{\mathbf{h}}(t)\}_{t\in\mathbb{R}_+}$ is the process $\{S^{(d)}_{\mathbf{h},J}(t)\}_{t\in\mathbb{R}_+}$ defined, for all $t \in \mathbb{R}_+$, by

$$S^{(d)}_{\mathbf{h},J}(t) = 2^{-J(h_1+\cdots+h_d-d+1)} \sum_{\mathbf{k}\in\mathcal{J}^1_J(t)} \sigma^{(\mathbf{h})}_{J,\mathbf{k}} \int_{\mathbb{R}} \prod_{\ell=1}^{d} \Phi_\Delta^{(h_\ell-1/2)}(s-k_\ell)\,ds. \tag{25}$$

REMARK 2.11. From consecutive uses of the Parseval–Plancherel identity and the inclusion (9), one can rewrite the integrals appearing in the right-hand side of (25) as integrals of compactly supported functions, see equation (33) below. This fact is particularly interesting for numerical computations.

The first main result of the present paper is that the sequence of simulation processes $(\{S^{(d)}_{\mathbf{h},J}(t)\}_{t\in\mathbb{R}_+})_{J\in\mathbb{N}}$ converges, almost surely and uniformly t belonging to any compact subset of $\mathbb{R}_+$, to the generalized Hermite process $\{X^{(d)}_{\mathbf{h}}(t)\}_{t\in\mathbb{R}_+}$ with the same estimate of the rate of convergence as the one established for the approximation process in Theorem 2.7.

THEOREM 2.12. *For any compact interval $I \subset \mathbb{R}_+$, there exists an almost surely finite random variable C (depending on I) for which one has, almost surely, for each $J \in \mathbb{N}$,*

$$\|X^{(d)}_{\mathbf{h}} - S^{(d)}_{\mathbf{h},J}\|_{I,\infty} \le C\,J^{\frac{d}{2}} 2^{-J(h_1+\cdots+h_d-d+1/2)}. \tag{26}$$

In order to state precisely the second main result of the present article, first we need to analyse carefully the definition of the set $D^1_J(t)$ in (19). To this end, for each fixed $J \in \mathbb{N}$ and $t \in \mathbb{R}_+$, we denote by $m_{J,t}$ the integer part of the real number $2^J t - 2^{J(1-a)}$, that is, $m_{J,t} := \lfloor 2^J t - 2^{J(1-a)} \rfloor$. Thus, in view of (19), it turns out that

$$D^1_J(t) = \begin{cases} \varnothing & \text{if } t \in [0, 2^{1-Ja}), \\ D^1_j(m_{J,t}2^{-J} + 2^{-Ja}) & \text{if } t \in [2^{1-Ja}, \infty). \end{cases} \tag{27}$$

Then, we can derive from (27) that the process $\{S^{(d)}_{\mathbf{h},J}(t)\}_{t\in\mathbb{R}^+}$ is a piecewise constant random function, that is a random walk. More precisely, if $\mathcal{I}_J$ stands for the set

$$\mathcal{I}_J := \mathbb{N} \cap [2^{J(1-a)}, +\infty),$$

one has

$$S^{(d)}_{\mathbf{h},J}(t) = \sum_{m\in\mathcal{I}_J} s_{m,J}\,\mathbb{1}_{\lambda^{(a)}_{m,J}}(t) \quad \text{for every } t \in \mathbb{R}_+, \tag{28}$$

where, for all $m \in \mathcal{I}_J$, the random variable

$$s_{m,J} := S^{(d)}_{\mathbf{h},J}\big(m2^{-J} + 2^{-aJ}\big) \tag{29}$$

and the deterministic bounded interval $\lambda^{(a)}_{m,J} := [m2^{-J} + 2^{-aJ}, (m+1)2^{-J} + 2^{-aJ})$.

In virtue of Theorem 2.12, when J is large enough, the random walk in (28) can be used for numerically simulating the generalized Hermite process $\{X^{(d)}_{\mathbf{h}}(t)\}_{t\in\mathbb{R}_+}$. Nevertheless, from Remark 2.2, we know that sample paths of the latter process are almost surely continuous functions. Thus, one could prefer to simulate them through a numerically computable stochastic process having continuous sample paths. This can be simply done by taking a

linear interpolation between the random points $(m2^{-J}+2^{-aJ}, s_{m,J})$, $m \in \mathcal{I}_J$. Namely, we consider the process $\{\widetilde{S}^{(d)}_{\mathbf{h},J}(t)\}_{t\in\mathbb{R}_+}$ defined, for all $t \in \mathbb{R}_+$, by

$$\begin{aligned}\widetilde{S}^{(d)}_{\mathbf{h},J}(t) &:= \frac{s_{m_0,J}}{|\lambda^{(a)}_{0,J}|} t \mathbb{1}_{\lambda^{(a)}_{0,J}}(t) \\ &\quad + \sum_{m\in\mathcal{I}_J} \big(2^J(s_{m+1,J}-s_{m,J})\big(t-\big(m2^{-J}+2^{-aJ}\big)\big)+s_{m,J}\big)\mathbb{1}_{\lambda_{m,J}}(t),\end{aligned} \tag{30}$$

with $m_0 := \min \mathcal{I}_J$, $\lambda^{(a)}_{0,J} := [0, m_0 2^{-J} + 2^{-aJ})$ and $|\lambda^{(a)}_{m_0,J}| = m_0 2^{-J} + 2^{-aJ}$.

The following theorem shows that the sequence of simulation processes $(\{\widetilde{S}^{(d)}_{\mathbf{h},J}(t)\}_{t\in\mathbb{R}_+})_{J\in\mathbb{N}}$ converges to $\{X^{(d)}_{\mathbf{h}}(t)\}_{t\in\mathbb{R}_+}$, almost surely and uniformly in t belonging to any compact interval of $\mathbb{R}_+$. Moreover, the estimate it provides for the almost uniform rate of convergence is the same as the one in Theorem 2.12.

THEOREM 2.13. *For any compact interval $I \subset \mathbb{R}_+$, there exists an almost surely finite random variable C' (depending on I) for which one has, almost surely, for each $J \in \mathbb{N}$,*

$$\big\|X^{(d)}_{\mathbf{h}} - \widetilde{S}^{(d)}_{\mathbf{h},J}\big\|_{I,\infty} \le C' J^{\frac{d}{2}} 2^{-J(h_1+\cdots+h_d-d+1/2)}.$$

REMARK 2.14. Before diving into the proofs of Theorems 2.12 and 2.13, let us emphasize that the estimate of the rate of convergence obtained in each one of them is identical to that previously established in Theorem 2.7. This, in some sense, means that we do not lose approximation quality when moving from the approximation process $\{X^{(d)}_{\mathbf{h},J}(t)\}_{t\in\mathbb{R}_+}$ to one or the other of the simulation processes $\{S^{(d)}_{\mathbf{h},J}(t)\}_{t\in\mathbb{R}_+}$ and $\{\widetilde{S}^{(d)}_{\mathbf{h},J}(t)\}_{t\in\mathbb{R}_+}$. Moreover, based on preliminary results, we believe that the estimate of the rate of convergence obtained in Theorems 2.7, 2.12 and 2.13 is (quasi)-optimal as soon as the order generalized Hermite process $d \ge 2$. Investigating this question will be the object of a forthcoming work.

3. Proofs of the main results.

3.1. *Proof of Theorem 2.12.* Our strategy to prove Theorem 2.12 consists in writing, for all $J \in \mathbb{N}$, the approximation error $X^{(d)}_{\mathbf{h}} - S^{(d)}_{\mathbf{h},J}$ as the sum of random variables, indexed by the sets $(D^1_J(t))^d$, $\mathcal{J}^1_J(t)$, $\mathcal{J}^2_J(t)$ and $\mathcal{J}^3_J(t)$ and to bound the sup-norm of these random variables in a suitable way. On this purpose, let us first remark that [5], Proposition 2.7, as well as [23], Lemma 2.2.17, allow to affirm the existence of C^* a positive finite random variable and Ω^* an event of probability 1, such that, on Ω^*, for all $J \in \mathbb{N}$ and $\mathbf{k} \in \mathbb{Z}^d$, one has

$$|\sigma^{(\mathbf{h})}_{J,\mathbf{k}}| \le C^* \prod_{\ell=1}^{d} \sqrt{\log(3+|J|+|k_\ell|)}. \tag{31}$$

LEMMA 3.1. *Let $T > 2$ be a fixed real number. There exists a positive almost surely finite random variable C such that, for all $J \in \mathbb{N}$, on Ω^*, the positive random variable*

$$\mathcal{G}^2_J := \sup_{t\in[0,T]} \left\{ 2^{-J(h_1+\cdots+h_d-d)} \sum_{\mathbf{k}\in\mathcal{J}^2_J(t)} |\sigma^{(\mathbf{h})}_{J,\mathbf{k}}| \left| \int_0^t \prod_{\ell=1}^{d} \Phi^{(h_\ell-1/2)}_{\Delta}(2^J s - k_\ell)\, ds \right| \right\}$$

is bounded from above by $C J^{\frac{d}{2}} (\log(3+J))^{\frac{d-1}{2}} 2^{-J(h_1+\cdots+h_d+a-d)}$.

PROOF. Let $L > 1$ be a fixed real number, for all $t \in [0, T]$, using the definition (23), the inequality (31) and the fast decay property (10), we have, on Ω^*,

$$2^{-J(h_1+\cdots+h_d-d)} \sum_{\mathbf{k}\in\mathcal{J}_J^2(t)} |\sigma_{J,\mathbf{k}}^{(\mathbf{h})}| \left| \int_0^t \prod_{\ell=1}^d \Phi_\Delta^{(h_\ell-1/2)}(2^J s - k_\ell)\, ds \right|$$

$$\leq C_1 \sup_{n\in[\![1,d]\!]} \left(2^{-J(h_1+\cdots+h_d-d)} \sum_{k_n\in D_J^2(t)} \sum_{\substack{k_\ell\in\mathbb{Z}\\ \ell\neq n}} \int_0^T \prod_{\ell=1}^d \frac{\sqrt{\log(3+J+|k_\ell|)}}{(3+|2^J s - k_\ell|)^L}\, ds \right),$$

where C_1 is a positive finite random variable, not depending on t or J. We proceed as in the proof of [5], Lemma 4.5, to get, on Ω^*,

$$|\mathcal{G}_J^2| \leq C_2 2^{-J(h_1+\cdots+h_d+a-d)} \sqrt{1+J} \log\big(3+J+2^J T\big)^{\frac{d-1}{2}}$$

$$\leq C_3 2^{-J(h_1+\cdots+h_d+a-d)} J^{\frac{d}{2}} \log(3+J)^{\frac{d-1}{2}},$$

where C_2 and C_3 are positive finite random variables, not depending on J. □

LEMMA 3.2. *Let $T > 2$ and $L \geq 2^{-1}(1-a)^{-1} + 1$ be two fixed real numbers. There exists a positive almost surely finite random variable C such that, for all $J \in \mathbb{N}$, on Ω^*, the positive random variable*

$$\mathcal{G}_J^3 := \sup_{t\in[0,T]} \left\{ 2^{-J(h_1+\cdots+h_d-d)} \sum_{\mathbf{k}\in\mathcal{J}_J^3(t)} |\sigma_{J,\mathbf{k}}^{(\mathbf{h})}| \left| \int_0^t \prod_{\ell=1}^d \Phi_\Delta^{(h_\ell-1/2)}(2^J s - k_\ell)\, ds \right| \right\}$$

is bounded from above by $C J^{\frac{d+1}{2}} (\log(3+J))^{\frac{d-1}{2}} 2^{-J(h_1+\cdots+h_d+(L-1)(1-a)-d)}$.

PROOF. For all $t \in [0, T]$, using the definition (24), the inequality (31) and the fast decay property (10), we have, on Ω^*,

$$2^{-J(h_1+\cdots+h_d-d)} \sum_{\mathbf{k}\in\mathcal{J}_J^3(t)} |\sigma_{J,\mathbf{k}}^{(\mathbf{h})}| \left| \int_0^t \prod_{\ell=1}^d \Phi_\Delta^{(h_\ell-1/2)}(2^J s - k_\ell)\, ds \right|$$

$$\leq C_1 \sup_{n\in[\![1,d]\!]} \left(2^{-J(h_1+\cdots+h_d-d)} \sum_{k_n\in D_J^3(t)} \sum_{\substack{k_\ell\in\mathbb{Z}\\ \ell\neq n}} \int_0^T \prod_{\ell=1}^d \frac{\sqrt{\log(3+J+|k_\ell|)}}{(3+|2^J s - k_\ell|)^L}\, ds \right),$$

where C_1 is a positive finite random variable, not depending on t or J. We proceed as in the proof of [5], Lemma 4.4, to get, on Ω^*,

$$|\mathcal{G}_J^3| \leq C_2 (1+J) \log\big(3+J+2^J T\big)^{\frac{d-1}{2}} 2^{-J(h_1+\cdots+h_d+(L-1)(1-a)-d)}$$

$$\leq C_3 J^{\frac{d+1}{2}} \log(3+J)^{\frac{d-1}{2}} 2^{-J(h_1+\cdots+h_d+(L-1)(1-a)-d)},$$

where C_2 and C_3 are positive finite random variables, not depending on J. □

LEMMA 3.3. *Let $T > 2$ and $L > 2$ be two fixed real numbers. There exists a positive almost surely finite random variable C such that, for all $J \in \mathbb{N}$, on Ω^*, the positive random variable*

$$\mathcal{G}_J^1 := \sup_{t\in[0,T]} \left\{ 2^{-J(h_1+\cdots+h_d-d)} \sum_{\mathbf{k}\in(D_J^1(t))^d} |\sigma_{J,\mathbf{k}}^{(\mathbf{h})}| \left| \int_{\mathbb{R}\setminus[0,t]} \prod_{\ell=1}^d \Phi_\Delta^{(h_\ell-1/2)}(2^J s - k_\ell)\, ds \right| \right\}$$

is bounded from above by $C J^{\frac{d}{2}} 2^{-J(d(L-1)(1-a)+h_1+\cdots+h_d-d+1)}$.

PROOF. For all $t \in [0,T]$, using the inequality (31), the fast decay property (10), the inequality $|k| \le 2^J T$, for all $k \in D_J^1(t)$, the inequality $2^J T \ge J$, [5], Lemma B.2, and the definition (19), we have, on Ω^*,

$$
\begin{aligned}
&2^{-J(h_1+\cdots+h_d-d)} \sum_{\mathbf{k}\in(D_J^1(t))^d} |\sigma_{J,\mathbf{k}}^{(\mathbf{h})}| \left| \int_{\mathbb{R}\setminus[0,t]} \prod_{\ell=1}^d \Phi_\Delta^{(h_\ell-1/2)}(2^J s - k_\ell)\, ds \right| \\
&\quad \le C_1 2^{-J(h_1+\cdots+h_d-d)} \int_{\mathbb{R}\setminus[0,t]} \prod_{\ell=1}^d \Bigg(\sum_{k_\ell\in D_J^1(t)} \frac{\sqrt{\log(3+J+|k_\ell|)}}{(3+|2^J s - k_\ell|)^L} \Bigg) ds \\
&\quad \le C_1 2^{-J(h_1+\cdots+h_d-d)} \int_{\mathbb{R}\setminus[0,t]} \prod_{\ell=1}^d \Bigg(\sum_{k_\ell\in D_J^1(t)} \frac{\sqrt{\log(3+2^{J+1}T)}}{(3+|2^J s - k_\ell|)^L} \Bigg) ds \\
&\quad \le C_2 J^{\frac{d}{2}} 2^{-J(h_1+\cdots+h_d-d)} \int_{\mathbb{R}\setminus[0,t]} \prod_{\ell=1}^d \Bigg(\sum_{k_\ell\in D_J^1(t)} \frac{1}{(3+|2^J s - k_\ell|)^L} \Bigg) ds \\
&\quad \le C_2 J^{\frac{d}{2}} 2^{-J(h_1+\cdots+h_d-d)} \big(I_J^1(t) + I_J^2(t) \big),
\end{aligned}
$$

where C_1 and C_2 are positive finite random variables, not depending on t or J, and we have set

$$
I_J^1(t) := \int_t^{+\infty} \prod_{\ell=1}^d \Bigg(\sum_{k_\ell \le 2^J t - 2^{J(1-a)}} \frac{1}{(3+2^J s - k_\ell)^L} \Bigg) ds
$$

and

$$
I_J^2(t) := \int_{-\infty}^0 \prod_{\ell=1}^d \Bigg(\sum_{k_\ell \ge 2^{J(1-a)}} \frac{1}{(3+k_\ell - 2^J s)^L} \Bigg) ds.
$$

In order to bound $I_J^1(t)$, we use the change of variable $y = 2^J(s-t)$ and the fact that the function $y \mapsto (2+y)^{-L}$ is decreasing on $\mathbb{R}_+$. By this way we obtain that

$$
\begin{aligned}
I_J^1(t) &= 2^{-J} \int_0^{+\infty} \prod_{\ell=1}^d \Bigg(\sum_{k_\ell \le 2^J t - 2^{J(1-a)}} \frac{1}{(3+y+2^J t - k_\ell)^L} \Bigg) dy \\
&\le 2^{-J} \int_0^{+\infty} \prod_{\ell=1}^d \Bigg(\int_0^{+\infty} \frac{dz}{(2+y+2^{J(1-a)}+z)^L} \Bigg) dy \\
&= 2^{-J} \int_0^{+\infty} \frac{(L-1)^{-d}}{(2+y+2^{J(1-a)})^{d(L-1)}}\, dy \\
&= 2^{-J} (L-1)^{-d} \big(d(L-1)-1 \big)^{-1} \big(2+2^{J(1-a)} \big)^{-(d(L-1)-1)}.
\end{aligned}
$$

We bound $I_J^2(t)$ in the same way and get the conclusion. □

To complete the proof Theorem 2.12, it only remains to bound the random variable

$$
2^{-J(h_1+\cdots+h_d-d+1)} \sum_{\mathbf{k}\in(D_J^1(t))^d \setminus \mathcal{J}_J^1(t)} \sigma_{J,\mathbf{k}}^{(\mathbf{h})} \int_{\mathbb{R}} \prod_{\ell=1}^d \Phi_\Delta^{(h_\ell-1/2)}(s-k_\ell)\, ds. \tag{32}
$$

To this end, we use the following key lemma.

LEMMA 3.4. *For all* $\mathbf{k} \in \mathbb{Z}^d$, *one has*

$$\int_{\mathbb{R}} \prod_{\ell=1}^{d} \Phi_{\Delta}^{(h_\ell - 1/2)}(s - k_\ell)\, ds = \int_{\mathbb{R}^{d-1}} e^{i(k_2-k_1)\xi} e^{i(k_3-k_2)\eta_3} \cdots e^{i(k_d-k_2)\eta_d} \times F(\xi, \eta_3, \ldots, \eta_d)\, d\xi\, d\eta_3 \cdots d\eta_d, \tag{33}$$

where F *is the function in the Schwartz class* $\mathcal{S}(\mathbb{R}^{d-1})$ *defined as follows*: *for all* $(\xi, \eta_3, \ldots, \eta_d) \in \mathbb{R}^{d-1}$,

$$F(\xi, \eta_3, \ldots, \eta_d) := (2\pi)^{-(d-1)} \widehat{\Phi_{\Delta}^{(h_1-1/2)}}(\xi) \times \overline{\widehat{\Phi_{\Delta}^{(h_2-1/2)}}\big(\xi - (\eta_3 + \cdots + \eta_d)\big)} \prod_{\ell=3}^{d} \overline{\widehat{\Phi_{\Delta}^{(h_\ell-1/2)}}}(\eta_\ell).$$

Moreover, since $F \in \mathcal{S}(\mathbb{R}^{d-1})$, *one can derive from* (33) *that*, *for each fixed* $L > 0$, *there exists a deterministic constant* $c_L > 0$ *for which the following is true*: *for all* $\mathbf{k} \in \mathbb{Z}^d$,

$$\left| \int_{\mathbb{R}} \prod_{\ell=1}^{d} \Phi_{\Delta}^{(h_\ell-1/2)}(s - k_\ell)\, ds \right| \le c_L \prod_{\ell=1, \ell\neq 2}^{d} \frac{1}{(1 + |k_\ell - k_2|)^L}. \tag{34}$$

PROOF. It follows from the change of variable $s = x + k_2$ that

$$\int_{\mathbb{R}} \prod_{\ell=1}^{d} \Phi_{\Delta}^{(h_\ell-1/2)}(s - k_\ell)\, ds = \int_{\mathbb{R}} \Phi_{\Delta}^{(h_1-1/2)}(x + k_2 - k_1) \times \Phi_{\Delta}^{(h_2-1/2)}(x) \prod_{\ell=3}^{d} \Phi_{\Delta}^{(h_\ell-1/2)}(x + k_2 - k_\ell)\, dx.$$

Then, using the Parseval–Plancherel identity and using $d-2$ times the equality[2] $\widehat{fg} = (2\pi)^{-1} \widehat{f} \star \widehat{g}$, for all $f, g \in \mathcal{S}(\mathbb{R})$, we get

$$\begin{aligned}
&\int_{\mathbb{R}} \Phi_{\Delta}^{(h_1-1/2)}(x + k_2 - k_1) \Phi_{\Delta}^{(h_2-1/2)}(x) \prod_{\ell=3}^{d} \Phi_{\Delta}^{(h_\ell-1/2)}(x + k_2 - k_\ell)\, dx \\
&= (2\pi)^{-1} \int_{\mathbb{R}} e^{i(k_2-k_1)\xi} \widehat{\Phi_{\Delta}^{(h_1-1/2)}}(\xi) \overline{\left(\widehat{\Phi_{\Delta}^{(h_2-1/2)} \prod_{\ell=3}^{d} \Phi_{\Delta}^{(h_\ell-1/2)}(\cdot + k_2 - k_\ell)} \right)}(\xi)\, d\xi \\
&= (2\pi)^{-(d-1)} \int_{\mathbb{R}} e^{i(k_2-k_1)\xi} \widehat{\Phi_{\Delta}^{(h_1-1/2)}}(\xi) \\
&\quad \times \overline{\big(\widehat{\Phi_{\Delta}^{(h_2-1/2)}} \star e^{i(k_2-k_3)(\cdot)} \widehat{\Phi_{\Delta}^{(h_3-1/2)}} \star \cdots \star e^{i(k_2-k_d)(\cdot)} \widehat{\Phi_{\Delta}^{(h_d-1/2)}} \big)}(\xi)\, d\xi \\
&= \int_{\mathbb{R}^{d-1}} e^{i(k_2-k_1)\xi} e^{i(k_3-k_2)\eta_3} \cdots e^{i(k_d-k_2)\eta_d} F(\xi, \eta_3, \ldots, \eta_d)\, d\xi\, d\eta_3 \cdots d\eta_d,
\end{aligned}$$

[2]Notice that throughout the article we use the convention that $\widehat{h} = \mathcal{F}(h)$ the Fourier transform of an arbitrary function $h \in \mathcal{S}(\mathbb{R})$ is defined as

$$\widehat{h}(t) = \mathcal{F}(h)(t) := \int_{\mathbb{R}} e^{-ity} h(y)\, dy \quad \text{for all } t \in \mathbb{R}.$$

Thus, $\mathcal{F}^{-1}(h)$, the inverse Fourier transform of h is defined as

$$\mathcal{F}^{-1}(h)(s) := (2\pi)^{-1} \int_{\mathbb{R}} e^{isz} h(z)\, dz \quad \text{for all } s \in \mathbb{R}.$$

which proves that the equality (33) holds. Let us now show that the inequality (34) is satisfied. Since F belongs to $\mathcal{S}(\mathbb{R}^{d-1})$, its Fourier transform $\widehat{F}$, defined, for all $(x_1,\dots,x_{d-1})\in\mathbb{R}^d$, as

$$\widehat{F}(x_1,\dots,x_{d-1}) := \int_{\mathbb{R}^{d-1}} e^{-i\langle (x_1,\dots,x_{d-1}),(\xi,\eta_3,\dots,\eta_d)\rangle} F(\xi,\eta_3,\dots,\eta_d)\,d\xi\,d\eta_3\cdots d\eta_d,$$

also belongs to the space $\mathcal{S}(\mathbb{R}^{d-1})$. Therefore, for each fixed $L>0$, there exists a deterministic constant $c_L>0$ such that

$$\sup_{(x_1,\dots,x_{d-1})\in\mathbb{R}^{d-1}} \bigl(1+|x_1|\bigr)^L\dots\bigl(1+|x_{d-1}|\bigr)^L\bigl|\widehat{F}(x_1,\dots,x_{d-1})\bigr| < c_L. \tag{35}$$

Thus, it turns out that the inequality (34) is a straightforward consequence of the equality (33) and the inequality (35). □

REMARK 3.5. The equality (33) can somehow be viewed as a useful extension of the well-known Parseval–Plancherel identity in which more than two functions are involved. In particular, it could have been used in Section 4.3 of our preceding paper [5] to get a more direct proof of Lemma 4.9 in the same spirit as [4], Lemma 2.21.

Lemma 3.4 is a main ingredient of the proof of the following lemma which allows to bound the random variable in (32).

LEMMA 3.6. *Let $T>2$ and $L>\max\{(2\varepsilon)^{-1},1\}$ be two fixed real numbers. There exists a positive almost surely finite random variable C such that, for all $J\in\mathbb{N}$, on Ω^*, the positive random variable*

$$\mathcal{G}_J := \sup_{t\in[0,T]}\left\{2^{-J(h_1+\cdots+h_d-d+1)}\sum_{\mathbf{k}\in(D_J^1(t))^d\setminus\mathcal{J}_J^1(t)}|\sigma_{J,\mathbf{k}}^{(\mathbf{h})}|\left|\int_{\mathbb{R}}\prod_{\ell=1}^d\Phi_\Delta^{(h_\ell-1/2)}(s-k_\ell)\,ds\right|\right\}$$

is bounded from above by $C\,J^{\frac{d}{2}}2^{-J(h_1+\cdots+h_d-d+\varepsilon L)}$.

PROOF. Let $t\in[0,T]$ and $\mathbf{k}\in(D_J^1(t))^d\setminus\mathcal{J}_J^1(t)$ be arbitrary and fixed. There is no restriction to assume that the coordinates $k_1,\dots,k_d$ of $\mathbf{k}$ are labeled so that $|k_1-k_2|>2^{\varepsilon J}$. Thus, using the inequality (34), we get

$$\left|\int_{\mathbb{R}}\prod_{\ell=1}^d\Phi_\Delta^{(h_\ell-1/2)}(s-k_\ell)\,ds\right| \le c_L 2^{-\varepsilon JL}\prod_{\ell=3}^d\frac{1}{(1+|k_\ell-k_2|)^L}.$$

Then, combining the latter inequality with (31) and the inequality $|k|\le 2^J T$, which holds for all $k\in D_J^1(t)$, we obtain

$$\begin{aligned}
&2^{-J(h_1+\cdots+h_d-d+1)}\sum_{\mathbf{k}\in(D_J^1(t))^d\setminus\mathcal{J}_J^1(t)}|\sigma_{J,\mathbf{k}}^{(\mathbf{h})}|\left|\int_{\mathbb{R}}\prod_{\ell=1}^d\Phi_\Delta^{(h_\ell-1/2)}(s-k_\ell)\,ds\right|\\
&\quad\le C_1 2^{-J(h_1+\cdots+h_d-d+1)}\bigl(\log(3+J+2^JT)\bigr)^{\frac{d}{2}}2^{-\varepsilon JL}\\
&\qquad\times\bigl(\#(D_J^1(t))\sup_{x\in\mathbb{R}}\Bigl(\sum_{k\in\mathbb{Z}}\frac{1}{(1+|k-x|)^L}\Bigr)^{d-2}\\
&\quad\le C_2 J^{\frac{d}{2}}2^{-J(h_1+\cdots+h_d-d+\varepsilon L)},
\end{aligned}$$

where $\#(D_J^1(t))$ denotes the cardinality of $D_J^1(t)$ which is less than $2^{J+1}T$, and C_1 and C_2 are positive finite random variable not depending on t or J. □

We are now in position to complete the proof of Theorem 2.12. Actually, it is a direct consequence of the Lemmata in this section and Theorem 2.7.

END OF THE PROOF OF THEOREM 2.12. Without loss of generality, one can assume that the compact interval I in the statement of the theorem is of the form $I = [0, T]$ for some fixed real number $T > 2$. Then, one can derive from the triangle inequality that, for all $J \in \mathbb{N}$,

$$\begin{aligned}\|X_{\mathbf{h}}^{(d)} - S_{\mathbf{h},J}^{(d)}\|_{I,\infty} &\leq \|X_{\mathbf{h}}^{(d)} - X_{\mathbf{h},J}^{(d)}\|_{I,\infty} + \|X_{\mathbf{h},J}^{(d)} - S_{\mathbf{h},J}^{(d)}\|_{I,\infty} \\ &\leq \|X_{\mathbf{h}}^{(d)} - X_{\mathbf{h},J}^{(d)}\|_{I,\infty} + \mathcal{G}_J^1 + \mathcal{G}_J^2 + \mathcal{G}_J^3 + \mathcal{G}_J.\end{aligned}$$

Then combining the latter inequality with Theorem 2.7 and Lemmata 3.1, 3.2, 3.3 and 3.6, one obtains Theorem 2.12. □

3.2. *Proof of Theorem 2.13.* We have now enough materials to complete the prove Theorem 2.13.

END OF THE PROOF OF THEOREM 2.13. For the sake of simpleness in notation, let us assume $I = [0, T]$, for some $T > 2$. In the sequel $J \in \mathbb{N}$ is arbitrary and fixed. The set of positive integers $\mathcal{I}_J(T)$ is defined as

$$\mathcal{I}_J(T) := \mathbb{N} \cap \left[2^{J(1-a)}, 2^J T - 2^{J(1-a)}\right] = \mathcal{I}_J \cap \left[0, 2^J T - 2^{J(1-a)}\right]. \tag{36}$$

One can derive from the triangle inequality that

$$\begin{aligned}\|S_{\mathbf{h},J}^{(d)} - \widetilde{S}_{\mathbf{h},J}^{(d)}\|_{I,\infty} &\leq \max\left\{|s_{m_0,J}|, \max_{m \in \mathcal{I}_J(T)} |s_{m+1,J} - s_{m,J}|\right\} \\ &\leq 2\|X_{\mathbf{h}}^{(d)} - S_{\mathbf{h},J}^{(d)}\|_{I,\infty} + \max\{A_J, B_J\},\end{aligned} \tag{37}$$

where

$$A_J := |X_{\mathbf{h}}^{(d)}(m_0 2^{-J} + 2^{-aJ}) - X_{\mathbf{h}}^{(d)}(0)|$$

and

$$B_J := \max_{m \in \mathcal{I}_J(T)} |X_{\mathbf{h}}^{(d)}((m+1)2^{-J} + 2^{-aJ}) - X_{\mathbf{h}}^{(d)}(m2^{-J} + 2^{-aJ})|.$$

Let γ be an arbitrary fixed positive real number such that $\gamma < H$ and $\gamma > a\gamma > H - \frac{1}{2}$. It follows from the inequality (8) that one has almost surely, for all $m \in \mathcal{I}_J(T)$,

$$|X_{\mathbf{h}}^{(d)}((m+1)2^{-J} + 2^{-aJ}) - X_{\mathbf{h}}^{(d)}(m2^{-J} + 2^{-aJ})| \leq C_{T,\gamma} 2^{-\gamma J}.$$

Then, combining the latter inequality with the fact that $\gamma > H - \frac{1}{2} = h_1 + \cdots + h_d - d + 1/2$, one obtains that

$$B_J \leq C_{T,\gamma} J^{\frac{d}{2}} 2^{-J(h_1+\cdots+h_d-d+1/2)}. \tag{38}$$

On another hand, since $m_0 2^{-J} + 2^{-aJ} \in I = [0, T]$ and $2^{J(1-a)} \leq m_0 < 2^{J(1-a)} + 1$, one can derive from the inequality (8) that, almost surely,

$$\begin{aligned}|X_{\mathbf{h}}^{(d)}(m_0 2^{-J} + 2^{-aJ}) - X_{\mathbf{h}}^{(d)}(0)| &\leq C_\gamma |m_0 2^{-J} + 2^{-aJ}|^\gamma \\ &\leq 3^\gamma C_{T,\gamma} 2^{-a\gamma J}.\end{aligned}$$

Then, using the inequality $a\gamma > H - \frac{1}{2}$, one gets that

$$A_J \leq 3^{\gamma} C_{T,\gamma} J^{\frac{d}{2}} 2^{-J(h_1+\cdots+h_d-d+1/2)}. \tag{39}$$

Finally, it follows from the triangle inequality, (37), (38) and (39) that

$$\begin{aligned}\big\|X_{\mathbf{h}}^{(d)} - \widetilde{S}_{\mathbf{h},J}^{(d)}\big\|_{I,\infty} &\leq \big\|X_{\mathbf{h}}^{(d)} - S_{\mathbf{h},J}^{(d)}\big\|_{I,\infty} + \big\|S_{\mathbf{h},J}^{(d)} - \widetilde{S}_{\mathbf{h},J}^{(d)}\big\|_{I,\infty} \\ &\leq 3\big\|X_{\mathbf{h}}^{(d)} - S_{\mathbf{h},J}^{(d)}\big\|_{I,\infty} + 4C_{T,\gamma} J^{\frac{d}{2}} 2^{-J(h_1+\cdots+h_d-d+1/2)}.\end{aligned}$$

Then combining the latter inequality with (26) one obtains the theorem. □

REMARK 3.7. Before ending the present section, let us provide a synthetic summary of our simulation method of trajectories (sample paths) of a generalized Hermite process with arbitrary order and Hurst parameter. We mention in passing that the sample paths of fractional Brownian motions, Rosenblatt processes, Hermite and generalized Hermite processes of order 3, which are displayed in Figures 1 to 7 of Section 4, have been obtained through this method.

The method depends on the following four parameters:

- the upper bound $T > 0$ of the interval $[0, T]$ on which the simulation of a trajectory is performed;
- the level of approximation $J \in \mathbb{N}$ (see Theorems 2.12 and 2.13);
- $a \in (1/2, 1)$ which determines the time set

$$\big\{m2^{-J} + 2^{-aJ} : m \in \mathcal{I}_J(T) \cup \big\{\max \mathcal{I}_J(T) + 1\big\}\big\}$$

on which data are simulated, recall that the finite set of positive integers $\mathcal{I}_J(T)$ is defined in (36), in the sequel one sets

$$m_0 := \min \mathcal{I}_J(T) = \min \mathcal{I}_J = \lceil 2^{J(1-a)} \rceil \quad \text{and} \quad m_1 := \max \mathcal{I}_J(T) = \lfloor 2^J T - 2^{J(1-a)} \rfloor;$$

- $\varepsilon > 0$ which governs, for any given $t \in \mathbb{R}_+$, the "thickness" of the set $\mathcal{J}_J^1(t)$ defined in (22).

We refer to Section 5.2 for a discussion on the role and the impact of these four parameters T, J, a and ε on the quality of the simulations.

For a given $J \in \mathbb{N}$ large enough so that the set $\mathcal{I}_J(T) = \{m_0, \ldots, m_1\}$ is nonempty, the method firstly consists to build the finite data set

$$\big\{s_{m,J} : m \in \{m_0, \ldots, m_1, m_1 + 1\}\big\}, \tag{40}$$

whose size (i.e., cardinality) is about $2^J T$, since

$$m_1 + 2 - m_0 = \lfloor 2^J T - 2^{J(1-a)} \rfloor + 2 - \lceil 2^{J(1-a)} \rceil \in \big[2^{J(1-a)} - 1, 2^J T - 2^{J(1-a)} + 1\big]. \tag{41}$$

Let us emphasize that for building this data set, we make use of an iterative procedure, since we know from (25) and (29) that

$$s_{m_0,J} := 2^{-J(h_1+\cdots+h_d-d+1)} \sigma_{J,\{m_0\}^d}^{(\mathbf{h})} \int_{\mathbb{R}} \prod_{\ell=1}^{d} \Phi_{\Delta}^{(h_\ell - 1/2)}(s - m_0)\, ds \tag{42}$$

and, for all $m \in \mathcal{I}_J$ (recall that $\{m_0, \ldots, m_1, m_1 + 1\} \subset \mathcal{I}_J$, see (36)),

$$s_{m+1,J} - s_{m,J} = 2^{-J(h_1+\cdots+h_d-d+1)} \sum_{\mathbf{k} \in \mathcal{J}_J^1[m]} \sigma_{J,\mathbf{k}}^{(\mathbf{h})} \int_{\mathbb{R}} \prod_{\ell=1}^{d} \Phi_{\Delta}^{(h_\ell - 1/2)}(s - k_\ell)\, ds, \tag{43}$$

where the finite set $\mathcal{J}_J^1[m]$ is defined as

$$\begin{aligned}\mathcal{J}_J^1[m] &:= \mathcal{J}_J^1\big((m+1)2^{-J}+2^{-aJ}\big)\setminus \mathcal{J}_J^1\big(m2^{-J}+2^{-aJ}\big)\\ &= \big\{\mathbf{k}\in\{\max\{m_0, m-\lfloor 2^{\varepsilon J}\rfloor\},\dots,m\}^d : \exists n \text{ such that } k_n = m\big\}.\end{aligned}$$

The method secondly consists to linearly interpolate the m_1+3-m_0 points whore coordinates are:

$$(0,0);\ \big(m_0 2^{-J}+2^{-aJ}, s_{m_0,J}\big);\ \dots;\ \big(m_1 2^{-J}+2^{-aJ}, s_{m_1,J}\big);\ \big((m_1+1)2^{-J}+2^{-aJ}, s_{m_1+1,J}\big).$$

By this way, we obtain a simulated continuous trajectory of a generalized Hermite process with arbitrary order and Hurst parameter on the interval $[0,(m_1+1)2^{-J}+2^{-aJ}]$ which contains the interval $[0,T]$.

Finally, the graph of the simulated trajectory is restricted to the interval $[0,T]$.

4. Examples. We use the process defined in (30) to numerically simulate the Rosenblatt process and the Hermite process of order 3. We refer to [40], Chapter 4, for more information on these processes. The significant parts of the algorithm we used to obtain these simulations are described in pseudo-code. Note that the practical implementation was carried out using a Python routine, which we make available to any interested reader.

4.1. *Simulation of the Rosenblatt process.* The Rosenblatt process of Hurst parameter $H\in(1/2,1)$ is the process introduced in (2) with $d=2$ and $\mathbf{h}=(1+\frac{H-1}{2},1+\frac{H-1}{2})$. To generate the random variables $(\sigma_{J,\mathbf{k}}^{(\mathbf{h})})_{J\in\mathbb{N},\mathbf{k}\in\mathbb{Z}^d}$, one can use the more explicit equation, derived from (12),

$$\sigma_{J,k_1,k_2}^{(1+\frac{H-1}{2},1+\frac{H-1}{2})} = Z_{J,k_1}^{(\frac{H}{2})}Z_{J,k_2}^{(\frac{H}{2})} - \mathbb{E}\big[Z_{J,k_1}^{(\frac{H}{2})}Z_{J,k_2}^{(\frac{H}{2})}\big], \tag{44}$$

where $(Z_{J,\ell}^{(\frac{H}{2})})_{\ell\in\mathbb{N}}$ is the Gaussian FARIMA $(0,\frac{H}{2},0)$ sequence associated to the sequence of Gaussian random variables $(2^{\frac{J}{2}}\int_{\mathbb{R}}\phi(2^J x-k)\,dB(x))_{k\in\mathbb{Z}}$. Note that we have [5], Remark 3.5, for all $J\in\mathbb{N}$ and $\mathbf{k}\in\mathbb{Z}^2$,

$$\mathbb{E}\big[Z_{J,k_1}^{(\frac{H}{2})}Z_{J,k_2}^{(\frac{H}{2})}\big] = \frac{1}{2\pi}\int_0^{2\pi} e^{i\xi(k_2-k_1)}\left|2\sin\left(\frac{\xi}{2}\right)\right|^{-H} d\xi. \tag{45}$$

On the other side, for all $\mathbf{k}\in\mathbb{Z}^2$, we get from the Definition 2.5 of the fractional scaling function and equation (33)

$$\int_{\mathbb{R}}\prod_{\ell=1}^{2}\Phi_{\Delta}^{(\frac{H}{2})}(s-k_\ell)\,ds = \int_{-\frac{4\pi}{3}}^{\frac{4\pi}{3}} e^{i\xi(k_2-k_1)}\left(\frac{\sin(\xi/2)}{\xi/2}\right)^H |\widehat{\phi}(\xi)|^2\,d\xi. \tag{46}$$

Note that the two expressions (44) and (46) are symmetric with respect to k_1 and k_2. Thus, in that case, one can rewrite the recursive formula (43) as

$$\begin{aligned}&s_{m+1,J}-s_{m,J}\\ &\quad= 2^{-JH}\big((Z_{J,m}^{(\frac{H}{2})})^2-\mathbb{E}[(Z_{J,m}^{(\frac{H}{2})})^2]\big)\int_{-\frac{4\pi}{3}}^{\frac{4\pi}{3}}\left(\frac{\sin(\xi/2)}{\xi/2}\right)^H|\widehat{\phi}(\xi)|^2\,d\xi\\ &\qquad+2\times 2^{-JH}\sum_{k=\max\{m_0,m-\lfloor 2^{\varepsilon J}\rfloor\}}^{m-1}\big(Z_{J,m}^{(\frac{H}{2})}Z_{J,k}^{(\frac{H}{2})}-\mathbb{E}[Z_{J,m}^{(\frac{H}{2})}Z_{J,k}^{(\frac{H}{2})}]\big)\\ &\qquad\times\int_{-\frac{4\pi}{3}}^{\frac{4\pi}{3}}e^{i\xi(m-k)}\left(\frac{\sin(\xi/2)}{\xi/2}\right)^H|\widehat{\phi}(\xi)|^2\,d\xi.\end{aligned}$$

Therefore, if $T>0$ is fixed and if:

1. `integralvector` is a vector of size $\lfloor 2^{\varepsilon J} \rfloor + 1$ such that, for all $0 \le k \le \lfloor 2^{\varepsilon J} \rfloor$, `integralvector`$[k]$ is the value of

$$\int_{-\frac{4\pi}{3}}^{\frac{4\pi}{3}} e^{i\xi k} \left(\frac{\sin(\xi/2)}{\xi/2} \right)^H |\widehat{\phi}(\xi)|^2 \, d\xi;$$

2. `IJ` is a vector containing $\mathcal{I}_J(T)$ with `IJ`$[0] = m_0$

3. `farima` contains a simulation of the random variables $(Z_{J,\ell}^{(\frac{H}{2})})_{\ell \in \mathcal{I}_J(T)}$;

4. `sigmaJ(farima,` $k_1, k_2, \frac{H}{2}$) is computing (44) using the simulation `farima` and the formula (45).

5. for all $m \in I_J(T)$, `epaissi(m)` is a vector of size $\min\{\lfloor 2^{\varepsilon J} \rfloor, m - m_0\} + 1$ such that, for all $0 \le i \le \min\{\lfloor 2^{\varepsilon J} \rfloor, m - m_0\}$, `epaissi(m)`$[i] = m - i$

the sequence $(s_{m,J})_{m \in \mathcal{I}_J(T)}$ is simulated via

ROSENBLATT(J)

```
result[0]=sigmaJ(farima,IJ[0],IJ[0],H/2) × integralvector[0]
for index=1 to length(IJ)
    element=epaissi(IJ[index])
    part=sigmaJ(farima,element[0],element[0],H/2) × integralvector[0]
    for i=1 to length(element)
        part=part+2 × sigmaJ(farima,element[0],element[i],H/2) × integralvector[i]
    result[index]=result[index-1]+part.
```

Indeed, it suffices to multiply the obtained vector result by 2^{-JH} to get a simulation of $(s_{m,J})_{m \in \mathcal{I}_J(T)}$.

The Figure 1 below shows four simulated sample paths of Rosenblatt processes of respective Hurst parameters 0.6; 0.7; 0.8 and 0.9 on the interval [0, 1]. They are obtained using our algorithm with parameters $J = 20$, $a = 0.99$ and $\varepsilon = 10^{-3}$ and $T = 1$. Note that, following the suggestion of one of the reviewers, the FARIMA sequence $(Z_{J,\ell}^{(\frac{H}{2})})_{\ell \in \mathcal{I}_J(T)}$ is simulated using a circulant matrix embedding method [14, 16, 18, 19, 54].

4.2. *Simulation of the Hermite process of order* 3. The Hermite process of order 3 and Hurst parameter $H \in (1/2, 1)$ is the process (2) with $d = 3$ and $\mathbf{h} = (1 + \frac{H-1}{3}, 1 + \frac{H-1}{3}, 1 +$

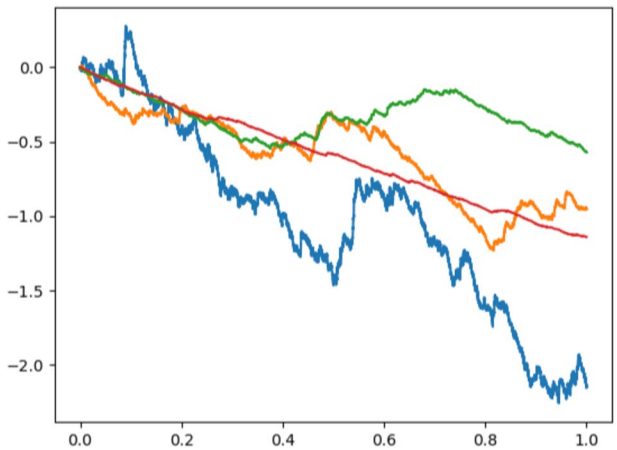

FIG. 1. *Sample paths of the Rosenblatt process of Hurst parameter* 0.6 (*blue*), 0.7 (*orange*), 0.8 (*green*) *and* 0.9 (*red*).

$\frac{H-1}{3}$). To generate the random variables $(\sigma_{J,\mathbf{k}}^{(\mathbf{h})})_{J\in\mathbb{N},\mathbf{k}\in\mathbb{Z}^d}$, one can use the more explicit equation, derived from (12),

$$
\begin{aligned}
&\sigma_{J,k_1,k_2,k_3}^{(1+\frac{H-1}{3},1+\frac{H-1}{3},1+\frac{H-1}{3})}\\
&\quad= Z_{J,k_1}^{(\frac{2H+1}{6})} Z_{J,k_2}^{(\frac{2H+1}{6})} Z_{J,k_3}^{(\frac{2H+1}{6})} - \mathbb{E}[Z_{J,k_1}^{(\frac{2H+1}{6})} Z_{J,k_2}^{(\frac{2H+1}{6})}] Z_{J,k_3}^{(\frac{2H+1}{6})}\\
&\qquad- \mathbb{E}[Z_{J,k_1}^{(\frac{2H+1}{6})} Z_{J,k_3}^{(\frac{2H+1}{6})}] Z_{J,k_2}^{(\frac{2H+1}{6})} - \mathbb{E}[Z_{J,k_2}^{(\frac{2H+1}{6})} Z_{J,k_3}^{(\frac{2H+1}{6})}] Z_{J,k_1}^{(\frac{2H+1}{6})},
\end{aligned}
\tag{47}
$$

where $(Z_{J,\ell}^{(\frac{2H+1}{6})})_{\ell\in\mathbb{N}}$ is the Gaussian FARIMA $(0, \frac{2H+1}{6}, 0)$ sequence associated to the sequence of Gaussian random variables $(2^{\frac{J}{2}} \int_{\mathbb{R}} \phi(2^J x - k)\, dB(x))_{k\in\mathbb{Z}}$. In this case, we have [5], Remark 3.5, for all $J \in \mathbb{N}$ and $k_1, k_2 \in \mathbb{Z}$,

$$
\mathbb{E}[Z_{J,k_1}^{(\frac{2H+1}{6})} Z_{J,k_2}^{(\frac{2H+1}{6})}] = \frac{1}{2\pi} \int_0^{2\pi} e^{i(k_2-k_1)} \left|2\sin\left(\frac{\xi}{2}\right)\right|^{-\frac{2H+1}{3}} d\xi.
\tag{48}
$$

Also, from the Definition 2.5 of the fractional scaling function and equation (33), we get, for all $\mathbf{k} \in \mathbb{Z}^3$,

$$
\begin{aligned}
&\int_{\mathbb{R}} \prod_{\ell=1}^{3} \Phi_{\Delta}^{(\frac{2H+1}{6})}(s - k_\ell)\, ds\\
&\quad= \iint_{[-\frac{4\pi}{3},\frac{4\pi}{3}]^2} e^{i\xi(k_2-k_1)} e^{i\eta(k_3-k_2)} \widehat{\phi}(\xi)\widehat{\phi}(\xi-\eta)\widehat{\phi}(\eta)\\
&\qquad\times \left(\frac{\sin(\xi/2)}{\xi/2} \frac{\sin((\xi-\eta)/2)}{(\xi-\eta)/2} \frac{\sin(\eta/2)}{\eta/2}\right)^{\frac{2H+1}{6}} d\xi\, d\eta.
\end{aligned}
\tag{49}
$$

Using again the symmetry of the expressions (47) and (49), we rewrite the recursive formula (43) in this context:

$$
\begin{aligned}
&s_{m+1,J} - s_{m,J}\\
&\quad= 2^{-JH}\Bigg[((Z_{J,m}^{(\frac{2H+1}{6})})^3 - 3\mathbb{E}[(Z_{J,m}^{(\frac{2H+1}{6})})^2](Z_{J,m}^{(\frac{2H+1}{6})}))\\
&\qquad\times \iint_{[-\frac{4\pi}{3},\frac{4\pi}{3}]^2} \widehat{\phi}(\xi)\widehat{\phi}(\xi-\eta)\widehat{\phi}(\eta)\left(\frac{\sin(\xi/2)}{\xi/2} \frac{\sin((\xi-\eta)/2)}{(\xi-\eta)/2} \frac{\sin(\eta/2)}{\eta/2}\right)^{\frac{2H+1}{6}} d\xi\, d\eta\Bigg]\\
&\qquad+ 3\times 2^{-JH} \sum_{k=\max\{m_0, m-\lfloor 2^{\varepsilon J}\rfloor\}}^{m-1} \Bigg[((Z_{J,m}^{(\frac{2H+1}{6})})^2 Z_{J,k}^{(\frac{2H+1}{6})} - \mathbb{E}[(Z_{J,m}^{(\frac{2H+1}{6})})^2] Z_{J,k}^{(\frac{2H+1}{6})}\\
&\qquad- 2\mathbb{E}[Z_{J,m}^{(\frac{2H+1}{6})} Z_{J,k}^{(\frac{2H+1}{6})}] Z_{J,m}^{(\frac{2H+1}{6})})\\
&\qquad\times \iint_{[-\frac{4\pi}{3},\frac{4\pi}{3}]^2} e^{i\eta(m-k)}\widehat{\phi}(\xi)\\
&\qquad\times \widehat{\phi}(\xi-\eta)\widehat{\phi}(\eta)\left(\frac{\sin(\xi/2)}{\xi/2} \frac{\sin((\xi-\eta)/2)}{(\xi-\eta)/2} \frac{\sin(\eta/2)}{\eta/2}\right)^{\frac{2H+1}{6}} d\xi\, d\eta\Bigg]\\
&\qquad+ 3\times 2^{-JH} \sum_{k=\max\{m_0, m-\lfloor 2^{\varepsilon J}\rfloor\}}^{m-1} \Bigg[((Z_{J,k}^{(\frac{2H+1}{6})})^2 Z_{J,m}^{(\frac{2H+1}{6})} - \mathbb{E}[(Z_{J,k}^{(\frac{2H+1}{6})})^2] Z_{J,m}^{(\frac{2H+1}{6})}
\end{aligned}
$$

$$
\begin{aligned}
&- 2\mathbb{E}\big[Z_{J,k}^{(\frac{2H+1}{6})} Z_{J,m}^{(\frac{2H+1}{6})}\big] Z_{J,k}^{(\frac{2H+1}{6})}\big) \\
&\times \iint_{[-\frac{4\pi}{3},\frac{4\pi}{3}]^2} e^{i\eta(m-k)} \widehat{\phi}(\xi) \\
&\times \widehat{\phi}(\xi-\eta)\widehat{\phi}(\eta)\bigg(\frac{\sin(\xi/2)}{\xi/2}\frac{\sin((\xi-\eta)/2)}{(\xi-\eta)/2}\frac{\sin(\eta/2)}{\eta/2}\bigg)^{\frac{2H+1}{6}} d\xi\, d\eta\bigg] \\
&+ 6\times 2^{-JH} \sum_{k=\max\{m_0,m-\lfloor 2^{\varepsilon J}\rfloor\}}^{m-1} \sum_{\ell=\max\{m_0,m-\lfloor 2^{\varepsilon J}\rfloor\}}^{k-1} \bigg[\big(Z_{J,m}^{(\frac{2H+1}{6})} Z_{J,k}^{(\frac{2H+1}{6})} Z_{J,\ell}^{(\frac{2H+1}{6})} \\
&- \mathbb{E}\big[Z_{J,m}^{(\frac{2H+1}{6})} Z_{J,k}^{(\frac{2H+1}{6})}\big] Z_{J,\ell}^{(\frac{2H+1}{6})} \\
&- \mathbb{E}\big[Z_{J,m}^{(\frac{2H+1}{6})} Z_{J,\ell}^{(\frac{2H+1}{6})}\big] Z_{J,k}^{(\frac{2H+1}{6})} \\
&- \mathbb{E}\big[Z_{J,k}^{(\frac{2H+1}{6})} Z_{J,\ell}^{(\frac{2H+1}{6})}\big] Z_{J,m}^{(\frac{2H+1}{6})}\big) \iint_{[-\frac{4\pi}{3},\frac{4\pi}{3}]^2} e^{i\xi(m-k)} e^{i\eta(k-\ell)} \\
&\times \widehat{\phi}(\xi)\widehat{\phi}(\xi-\eta)\widehat{\phi}(\eta)\bigg(\frac{\sin(\xi/2)}{\xi/2}\frac{\sin((\xi-\eta)/2)}{(\xi-\eta)/2}\frac{\sin(\eta/2)}{\eta/2}\bigg)^{\frac{2H+1}{6}} d\xi\, d\eta\bigg].
\end{aligned}
$$

Therefore, if $T>0$ is fixed and if:

1. `integralmatrix` is a matrix of dimension $\lfloor 2^{\varepsilon J}\rfloor+1$ such that, for all $0\le k,\ell\le \lfloor 2^{\varepsilon J}\rfloor$, `integralmatrix`$[k,l]$ is the value of

$$\iint_{[-\frac{4\pi}{3},\frac{4\pi}{3}]^2} e^{i\xi k} e^{i\eta\ell}\widehat{\phi}(\xi)\widehat{\phi}(\xi-\eta)\widehat{\phi}(\eta)\bigg(\frac{\sin(\xi/2)}{\xi/2}\frac{\sin((\xi-\eta)/2)}{(\xi-\eta)/2}\frac{\sin(\eta/2)}{\eta/2}\bigg)^{\frac{2H+1}{6}} d\xi\, d\eta$$

2. `IJ` is a vector containing $\mathcal{I}_J(T)$ with `IJ`$[0]=m_0$
3. `farima` contains a simulation of the random variables $(Z_{J,\ell}^{(\frac{2H+1}{6})})_{\ell\in\mathcal{I}_J(T)}$;
4. `sigmaJ(farima,`$k_1,k_2,k_3,\frac{2H+1}{6}$`)` is computing (47) using the simulation `farima` and the formula (48).
5. for all $m\in I_J(T)$, `epaissi(m)` is a vector of size $\min\{\lfloor 2^{\varepsilon J}\rfloor, m-m_0\}+1$ such that, for all $0\le i\le \min\{\lfloor 2^{\varepsilon J}\rfloor, m-m_0\}$, `epaissi(m)`$[i]=m-i$

the sequence $(s_{m,J})_{m\in\mathcal{I}_J(T)}$ is simulated via

HERMITE3(J)

```
1  result[0]=sigmaJ(farima,IJ[0],IJ[0],IJ[0],2H+1/6) × integralmatrix[0,0]
2  for index=1 to length(IJ)
3      element=epaissi(IJ[index])
4      part=sigmaJ(farima,element[0],element[0],element[0],2H+1/6) × integralmatrix[0,0]
5      for i=1 to length(element)
6          part=part+3 × sigmaJ(farima,element[0],element[0],element[i],2H+1/6) × integralmatrix[0,i]
7          part=part+3 × sigmaJ(farima,element[0],element[i],element[i],2H+1/6) × integralmatrix[0,i]
8          for j=i+1 to length(element)
9              part=part+6 × sigmaJ(farima,element[0],element[i],element[j],2H+1/6) × integralmatrix[i,j-i]
10     result[index]=result[index-1]+part.
```

Indeed, it suffices to multiply the obtained vector result by 2^{-JH} to get a simulation of $(s_{m,J})_{m\in\mathcal{I}_J(T)}$.

The Figure 2 below shows four simulated sample paths of Hermite processes of order 3 and respective Hurst parameter 0.6; 0.7; 0.8 and 0.9 on the interval [0, 1]. They are obtained using our algorithm again with parameters $J=20$, $a=0.99$ and $\varepsilon=10^{-3}$ and $T=1$. The

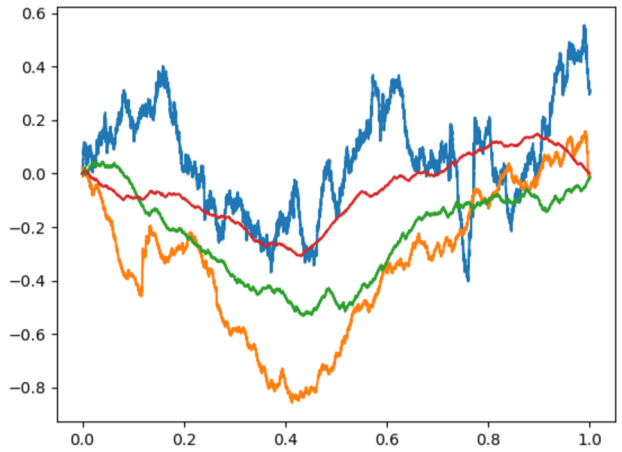

FIG. 2. *Sample paths of the Hermite process of order* 3 *of Hurst parameter* 0.6 (*blue*), 0.7 (*orange*), 0.8 (*green*) *and* 0.9 (*red*).

FARIMA sequence $(Z_{J,\ell}^{(\frac{2H+1}{6})})_{\ell\in\mathcal{I}_J(T)}$ is once again computed via a circulant matrix embedding method.

Of course, our algorithm can also be used to simulate sample paths of the fractional Brownian motion with Hurst parameter $H \in (1/2, 1)$. In this context, the integrals appearing both in the definitions of $\{S_{\mathbf{h},J}^{(d)}(t)\}_{t\in\mathbb{R}_+}$ and $\{\widetilde{S}_{\mathbf{h},J}^{(d)}(t)\}_{t\in\mathbb{R}_+}$ are all equal to 1. Thus, the approximation scheme, consisting in summing terms of the Gaussian FARIMA sequence $(Z_{J,\ell}^{(H-\frac{1}{2})})_{\ell\in\mathbb{N}}$, according to the sets $(\mathcal{J}_J^1(m2^{-J}+2^{-aJ}))_{m\in\mathcal{I}_J}$ is particularly elementary to implement. In the Figures 3, 4, 5 and 6 below, we compare simulated sample paths of the fractional Brownian, the Rosenblatt process and the Hermite process of order 3, with Hurst parameter 0.6; 0.7; 0.8 and 0.9. All simulations are once again obtained using our algorithm with parameters $J = 20$, $a = 0.99$ and $\varepsilon = 10^{-3}$.

REMARK 4.1. To get the simulations in Figures 3, 4, 5, 6, we use the standard normalisation of Hermite processes (see Remark 2.3 above) which is more appropriate to compare the sample paths.

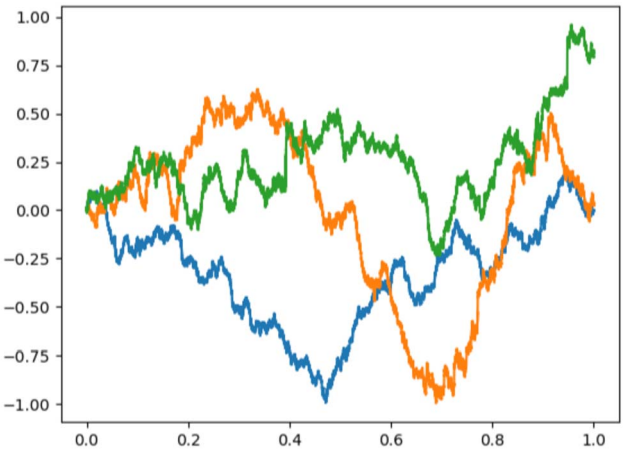

FIG. 3. *Sample paths of the fractional Brownian Motion* (*blue*), *the Rosenblatt process* (*orange*) *and the Hermite process of order* 3 (*green*) *with Hurst parameter* 0.6.

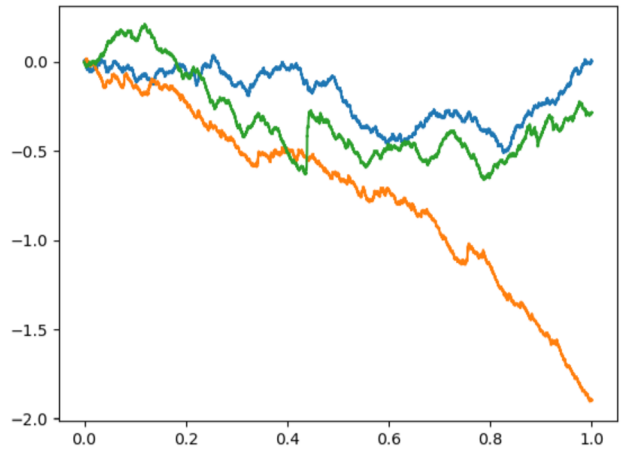

FIG. 4. *Sample paths of the fractional Brownian Motion* (*blue*), *the Rosenblatt process* (*orange*) *and the Hermite process of order* 3 (*green*) *with Hurst parameter* 0.7.

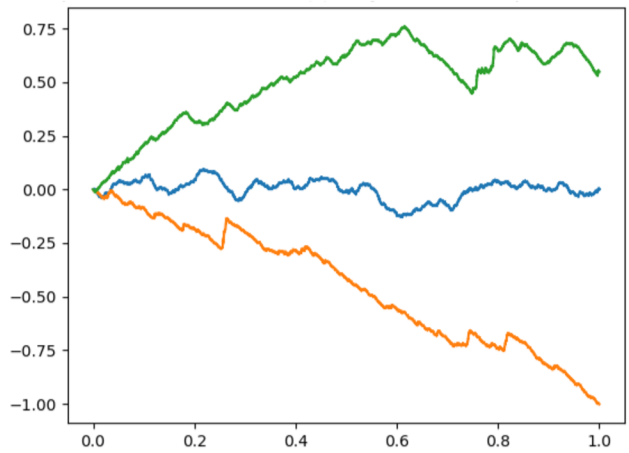

FIG. 5. *Sample paths of the fractional Brownian Motion* (*blue*), *the Rosenblatt process* (*orange*) *and the Hermite process of order* 3 (*green*) *with Hurst parameter* 0.8.

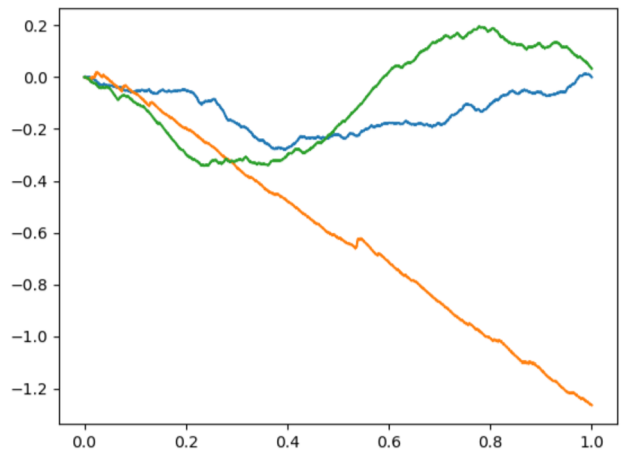

FIG. 6. *Sample paths of the fractional Brownian Motion* (*blue*), *the Rosenblatt process* (*orange*) *and the Hermite process of order* 3 (*green*) *with Hurst parameter* 0.9.

4.3. *Simulation of the generalized Hermite process of order* 3. Our approach can also be used to numerically simulate generalized Hermite processes. We consider here the case of a process of order $d = 3$ and arbitrary $\mathbf{h} = (h_1, h_2, h_3)$ satisfying conditions (3). To generate the random variables $(\sigma_{J,\mathbf{k}}^{(\mathbf{h})})_{J\in\mathbb{N},\mathbf{k}\in\mathbb{Z}^d}$, we use the more explicit equation, derived from (12),

$$\begin{aligned}
&\sigma_{J,k_1,k_2,k_3}^{(h_1,h_2,h_3)}\\
&\quad= Z_{J,k_1}^{(h_1-1/2)} Z_{J,k_2}^{(h_2-1/2)} Z_{J,k_3}^{(h_3-1/2)} - \mathbb{E}\big[Z_{J,k_1}^{(h_1-1/2)} Z_{J,k_2}^{(h_2-1/2)}\big] Z_{J,k_3}^{(h_3-1/2)}\\
&\qquad- \mathbb{E}\big[Z_{J,k_1}^{(h_1-1/2)} Z_{J,k_3}^{(h_3-1/2)}\big] Z_{J,k_2}^{(h_2-1/2)} - \mathbb{E}\big[Z_{J,k_2}^{(h_2-1/2)} Z_{J,k_3}^{(h_3-1/2)}\big] Z_{J,k_1}^{(h_1-1/2)},
\end{aligned} \tag{50}$$

where, for any $\ell \in \{1, 2, 3\}$, $(Z_{J,\ell}^{(h_\ell-1/2)})_{\ell\in\mathbb{N}}$ is the Gaussian FARIMA $(0, h_\ell - 1/2, 0)$ sequence associated to the sequence of Gaussian random variables $(2^{\frac{J}{2}} \int_{\mathbb{R}} \phi(2^J x - k) \times dB(x))_{k\in\mathbb{Z}}$. In this case, we use again [5], Remark 3.5, to compute, for all $J \in \mathbb{N}$, $\ell, m \in \{1, 2, 3\}$ and $k_\ell, k_m \in \mathbb{Z}$,

$$\begin{aligned}
&\mathbb{E}\big[Z_{j,k_\ell}^{(h_\ell-1/2)} Z_{j,k_m}^{(h_m-1/2)}\big]\\
&\quad= \frac{1}{2\pi} \int_0^{2\pi} e^{i(k_\ell-k_m)\xi} \big(1 - e^{-i\xi}\big)^{-(h_\ell-1/2)} \big(1 - e^{i\xi}\big)^{-(h_m-1/2)}\, d\xi.
\end{aligned} \tag{51}$$

Also, from the Definition 2.5 of the fractional scaling function and equation (33), we get, for all $\mathbf{k} \in \mathbb{Z}^3$,

$$\begin{aligned}
&\int_{\mathbb{R}} \prod_{\ell=1}^{3} \Phi_\Delta^{(h_\ell-1/2)}(s - k_\ell)\, ds\\
&\quad= \iint_{[-\frac{4\pi}{3},\frac{4\pi}{3}]^2} e^{i\xi(k_2-k_1+h_2-h_1)} e^{i\eta(k_3-k_2+h_3-h_2)} \widehat{\phi}(\xi)\\
&\qquad\times \widehat{\phi}(\xi-\eta)\widehat{\phi}(\eta) \left(\frac{\sin(\xi/2)}{\xi/2}\right)^{(h_1-1/2)}\\
&\qquad\times \cdots \times \left(\frac{\sin((\xi-\eta)/2)}{(\xi-\eta)/2}\right)^{(h_2-1/2)} \left(\frac{\sin(\eta/2)}{\eta/2}\right)^{(h_3-1/2)} d\xi\, d\eta.
\end{aligned} \tag{52}$$

Now, the expressions (50) and (52) are not symmetric, which means that we have to compute much more quantities in our algorithm. Indeed, if $T > 0$ is fixed and if:

1. `integralmatrix` is a matrix of dimension $2 \times \lfloor 2^{\varepsilon J} \rfloor + 1$ such that, for all $-\lfloor 2^{\varepsilon J} \rfloor \le k, \ell \le \lfloor 2^{\varepsilon J} \rfloor$, `integralmatrix`$[k, l]$ is the value of

$$\begin{aligned}
&\iint_{[-\frac{4\pi}{3},\frac{4\pi}{3}]^2} e^{i\xi(k+h_2-h_1)} e^{i\eta(\ell+h_3-h_2)} \widehat{\phi}(\xi)\widehat{\phi}(\xi-\eta)\widehat{\phi}(\eta) \left(\frac{\sin(\xi/2)}{\xi/2}\right)^{(h_1-1/2)}\\
&\quad\times \cdots \times \left(\frac{\sin((\xi-\eta)/2)}{(\xi-\eta)/2}\right)^{(h_2-1/2)} \left(\frac{\sin(\eta/2)}{\eta/2}\right)^{(h_3-1/2)} d\xi\, d\eta.
\end{aligned}$$

2. `IJ` is a vector containing $\mathcal{I}_J(T)$ with `IJ`$[0] = m_0$
3. for any $\ell \in \{1, 2, 3\}$, f_ℓ contains a simulation of the random variables $(Z_{J,m}^{(h_\ell-1/2)})_{m\in\mathcal{I}_J(T)}$;
4. `sigmaJ`$(f_1, f_2, f_3, k_1, k_2, k_3, \mathbf{h})$ is computing (50) using the three simulations f_1, f_2, f_3 and the formula (51).
5. for all $m \in I_J(T)$, `epaissi`$(\mathtt{m})$ is a vector of size $\min\{\lfloor 2^{\varepsilon J} \rfloor, m - m_0\} + 1$ such that, for all $0 \le i \le \min\{\lfloor 2^{\varepsilon J} \rfloor, m - m_0\}$, `epaissi`$(\mathtt{m})[i] = m - i$

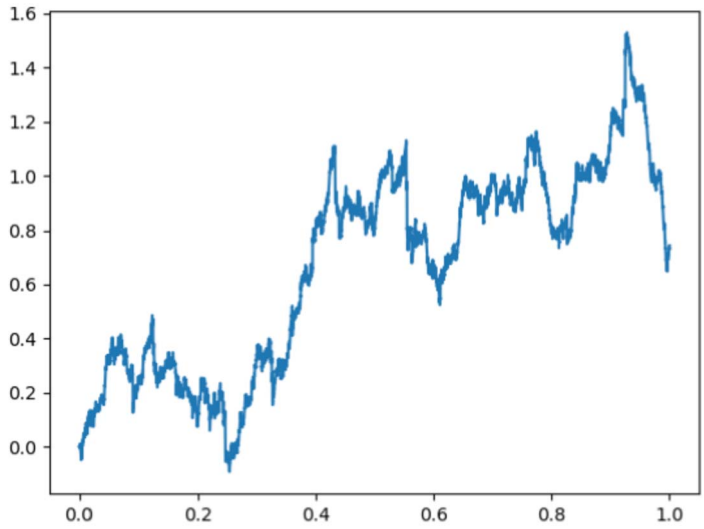

FIG. 7. *Sample path of the generalized Hermite of order* 3 *with index* $\mathbf{h} = (0.8, 0.85, 0.9)$.

the sequence $(s_{m,J})_{m\in\mathcal{I}_J(T)}$ is simulated via

GENHERMITE3(J)

```
result[0]=sigmaJ(f1,f2,f3,IJ[0],IJ[0],IJ[0],h) × integralmatrix[0,0]
for index=1 to length(IJ)
    element=epaissi(IJ[index])
    part=sigmaJ(f1,f2,f3,element[0],element[0],element[0],h) × integralmatrix[0,0]
    for i=1 to length(element)
        part=part+ sigmaJ(f1,f2,f3,element[0],element[0],element[i],h) × integralmatrix[0,-i]
        part=part+ sigmaJ(f1,f2,f3,element[0],element[i],element[0],h) × integralmatrix[-i,i]
        part=part+ sigmaJ(f1,f2,f3,element[i],element[0],element[0],h) × integralmatrix[i,0]
        part=part+ sigmaJ(f1,f2,f3,element[0],element[i],element[i],h) × integralmatrix[-i,0]
        part=part+ sigmaJ(f1,f2,f3,element[i],element[0],element[i],h) × integralmatrix[i,-i]
        part=part+ sigmaJ(f1,f2,f3,element[i],element[i],element[0],h) × integralmatrix[0,i]
        for j=1 to length(element)
            if j ≠ i
                part=part+ sigmaJ(f1,f2,f3,element[0],element[i],element[j],h) × integralmatrix[-i,j-i]
                part=part+ sigmaJ(f1,f2,f3,element[0],element[j],element[i],h) × integralmatrix[-j,j-i]
                part=part+ sigmaJ(f1,f2,f3,element[i],element[0],element[j],h) × integralmatrix[i,-j]
                part=part+ sigmaJ(f1,f2,f3,element[j],element[0],element[i],h) × integralmatrix[j,-i]
                part=part+ sigmaJ(f1,f2,f3,element[i],element[j],element[0],h) × integralmatrix[i-j,j]
                part=part+ sigmaJ(f1,f2,f3,element[j],element[i],element[0],h) × integralmatrix[j-i,i]
    result[index]=result[index-1]+part.
```

Due to the numerous additional computations, this algorithm clearly needed more time to produce a simulation than its counterpart for the usual Hermite process of order 3. For this reason, the sample path displayed in Figure 7 above is obtained with $J = 15$ (instead of $J = 20$ in the previous figures). The other parameters are $h_1 = 0.8$; $h_2 = 0.85$ and $h_3 = 0.9$, $a = 0.75$ and $\varepsilon = 10^{-3}$.

5. Some numerical experiments.

5.1. *Validation of the trajectories.* To numerically validate our simulations, we propose to estimate their Hurst parameter using three well-established methods:

- the local Whittle estimators (LW) [26, 33, 42]
- log-variogram estimations (LV) [3, 10, 12]
- quadratic-variation estimators (QV). [6]

TABLE 1
LW estimations of the Hurst parameter

		0.6	0.7	0.8	0.9
FBM	m	0.600	0.699	0.799	0.899
	s	0.004	0.004	0.004	0.004
RP	m	0.656	0.725	0.801	0.878
	s	0.008	0.011	0.014	0.012
HP	m	0.656	0.717	0.790	0.901
	s	0.017	0.017	0.012	0.010

Tables 1 to 3 below presented the Hurst parameter estimations obtained for the fractional Brownian motion (FBM), Rosenblatt process (RP) and Hermite process of order 3 (HP) simulated with prescribed Hurst parameter 0.6, 0.7, 0.8 and 0.9. In each case, we simulated 100 trajectories with $J = 17$, $a = 0.99$ and $\varepsilon = 10^{-3}$ and $T = 1$. The notation m and s stand respectively for the mean of the estimations and their standard deviation. Figure 8 displays the 1,200 trajectories obtained from this numerical experiment.

These numerical experiments seem to support the idea that the simulated trajectories exhibit a reasonably good Hurst index. This was already apparent from Figures 1 to 6 above: the larger H is, the smoother the trajectories become.

REMARK 5.1. In this analysis, we have chosen to work with the modified quadratic variation estimator defined in [6], so that the asymptotic performance of the estimator does not depend on the exact value of the Hurst parameter H or on the order d of the process. Indeed, it is known that the classical Hurst index estimator based on quadratic variations, although strongly consistent, is not asymptotically Gaussian as soon as $d \geq 2$, and even at order $d = 1$ provided that $H > \frac{3}{4}$ [11, 51]. The estimator recently introduced in [6] has the advantage of overcoming this issue and is therefore asymptotically normal in all cases. Note, however, that given an observation of a process $\{X_{\frac{k}{2^N}} : 0 \leq k \leq 2^N\}$ on a dyadic grid, this modified estimator is obtained by considering only the increments $\{X_{\frac{\ell[2^{N\beta}]+1}{2^N}} - X_{\frac{\ell[2^{N\beta}]}{2^N}} : \ell \in \mathbb{N} \cap [1, \min\{[2^{N\gamma}], \frac{2^N}{[2^{N\beta}]}\}]\}$, for some $0 < \gamma < \beta < 1$, so as to ensure that the intervals associated to these increments are sufficiently far apart to define random variables which possess independence properties. In other words, the modified estimator uses only part of the information available in $\{X_{\frac{k}{2^N}} : 0 \leq k \leq 2^N\}$, which naturally slows its rate of convergence to H, see [6], Theorem 3. In this work, for comparative purposes, we

TABLE 2
LV estimations of the Hurst parameter

		0.6	0.7	0.8	0.9
FBM	m	0.594	0.692	0.787	0.886
	s	0.010	0.013	0.013	0.015
RP	m	0.638	0.702	0.779	0.850
	s	0.018	0.023	0.029	0.029
HP	m	0.636	0.703	0.792	0.915
	s	0.017	0.016	0.013	0.015

TABLE 3
QV estimations of the Hurst parameter

		0.6	0.7	0.8	0.9
FBM	m	0.605	0.705	0.806	0.904
	s	0.006	0.005	0.006	0.007
RP	m	0.585	0.693	0.796	0.896
	s	0.013	0.013	0.015	0.012
HP	m	0.586	0.691	0.802	0.896
	s	0.031	0.026	0.016	0.006

considered it more appropriate to guarantee the same asymptotic properties of the estimator regardless of the values of d and H, even at the cost of slightly slowing its convergence.

REMARK 5.2. In the paper [28], numerical experiments are carried out to test the performance of a wavelet-based estimator for the Hust parameter of a Hermite process. Therein, as well as in the initial version of the current article, trajectories of this process were simulated through FARIMAs generated by a wavelet synthesis similar to that presented in [1, 39]. Yet, a referee on the initial version of our paper suggested us to use a circulant matrix embedding algorithm to generate them, since it offers the advantage to be an exact method. This sensible suggestion has been followed in the present revised version of the paper. Indeed, it allows to greatly improve the results of the numerical experiments. For instance, a comparison of the estimations in Table 4 with the ones presented in [28] clearly confirms this fact.

Another fundamental aspect of the Hermite processes is their non-Gaussianity as soon as $d \geq 2$. Recall that our trajectories on $[0, 1]$ are obtained by simulating data at the times $m2^{-J} + 2^{-aJ}$, $m \in \mathcal{I}_J(1)$, for a given $J \in \mathbb{N}$ (see Remark 3.7). In the sequel, $\mathcal{D}_J$ stands for

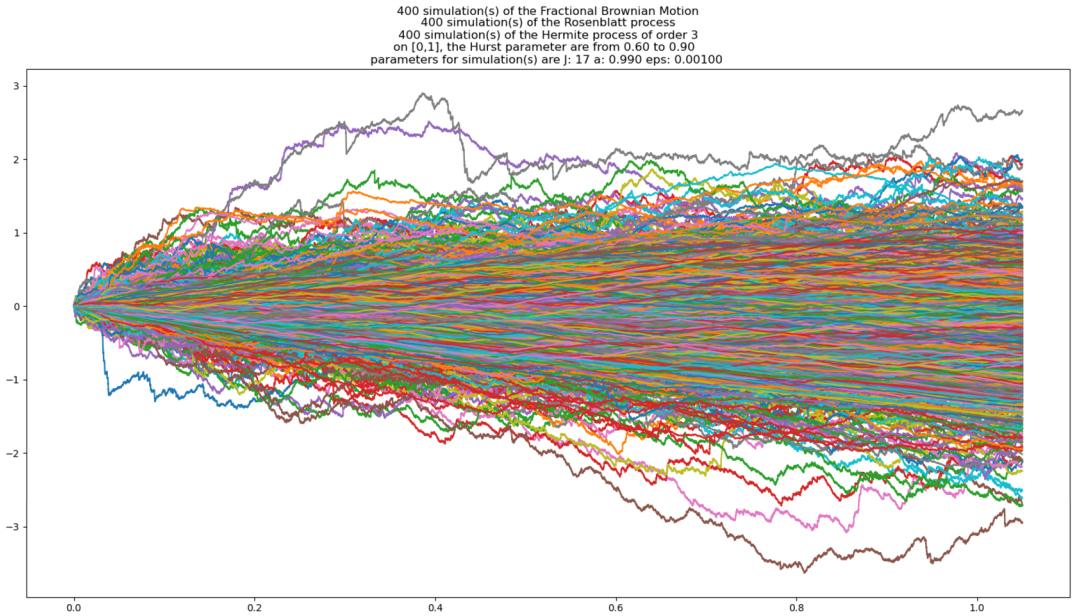

FIG. 8. *The* 1,200 *trajectories generated to obtain the estimations presented in Tables* 1 *to* 4.

TABLE 4
WV estimations of the Hurst parameter

		0.6	0.7	0.8	0.9
FBM	m	0.620	0.713	0.807	0.903
	s	0.177	0.156	0.168	0.169
RP	m	0.630	0.713	0.759	0.886
	s	0.187	0.205	0.230	0.244
HP	m	0.623	0.695	0.794	0.883
	s	0.266	0.219	0.207	0.218

the set $\mathcal{I}_J(1) \setminus \{m_0\}$. For any $J \in \mathbb{N}$, $d \geq 1$, $H \in (1/2, 1)$ and $m \in \mathcal{D}_J$, the random variable $X^{(d)}_{H,m,J}$ is defined as

$$X^{(d)}_{H,m,J} := 2^{JH}\big(X^{(d)}_H\big(m2^{-J} + 2^{-aJ}\big) - X^{(d)}_H\big((m-1)2^{-J} + 2^{-aJ}\big)\big),$$

where $\{X^{(d)}_H(t)\}_{t\geq 0}$ denotes the Hermite process of order d and Hurst parameter H. The empirical cumulative distribution function $\widehat{F}^{(d)}_{H,J}$ is defined, for all $x \in \mathbb{R}$, as

$$\widehat{F}^{(d)}_{H,J}(x) := \frac{1}{\#\mathcal{D}_J} \sum_{m\in\mathcal{D}_J} \mathbb{1}_{\{X^{(d)}_{H,m,J} \leq x\}},$$

where $\#\mathcal{D}_J$ denotes the cardinality of $\mathcal{D}_J$. On another hand, the cumulative distribution function $F^{(d)}_H$ is defined, for every $x \in \mathbb{R}$, as

$$F^{(d)}_H(x) := \mathbb{P}\big(X^{(d)}_H(1) \leq x\big).$$

The following proposition is the theoretical foundation behind our empirical approach to test the Gaussianity of the simulated processes.

PROPOSITION 5.3. *For each fixed integer $d \geq 1$ and $H \in (1/2, 1)$, the sequence of functions $(\widehat{F}^{(d)}_{H,J})_{J\in\mathbb{N}}$ converges, almost surely and uniformly in $x \in \mathbb{R}$, to the function $F^{(d)}_H$.*

PROOF. We know from [44], Theorem 8.3.1, that the stationary Hermite noise $(X^{(d)}_H(m) - X^{(d)}_H(m-1))_{m\in\mathbb{N}}$ is ergodic. Thus, one can derive from the self-similarity property of the process $\{X^{(d)}_H(t)\}_{t\geq 0}$ the stationarity of its increments that

$$\text{for all } x \in \mathbb{R} \quad \mathbb{P}\Big(\lim_{J\to+\infty} \widehat{F}^{(d)}_{H,J}(x) = F^{(d)}_H(x)\Big) = 1.$$

Then, since $\mathbb{Q}$ is a countable set, one gets that

$$\mathbb{P}\Big(\forall x \in \mathbb{Q}, \lim_{J\to+\infty} \widehat{F}^{(d)}_{H,J}(x) = F^{(d)}_H(x)\Big) = 1.$$

Next, we use the facts that $\mathbb{Q}$ is dense in $\mathbb{R}$ and $x \mapsto \widehat{F}^{(d)}_{H,J}(x)$ is almost surely nondecreasing to obtain that

$$\mathbb{P}\Big(\forall x \in \mathbb{R}, \lim_{J\to+\infty} \widehat{F}^{(d)}_{H,J}(x) = F^{(d)}_H(x)\Big) = 1. \tag{53}$$

Next, notice that since the random variable $X^{(d)}_H(1)$ can be expressed as a nonzero multiple Wiener–Itô integral, we know from the Shigekawa theorem [46] that its distribution is absolutely continuous with respect to the Lebesgue measure on $\mathbb{R}$. The latter fact entails that $F^{(d)}_H$

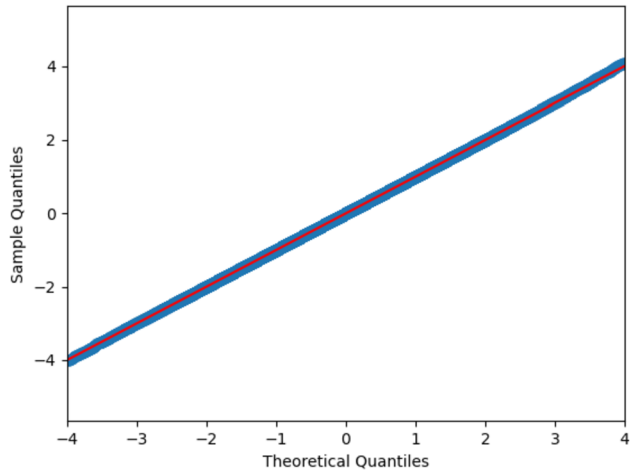

FIG. 9. *Qq-plot comparing the empirical quantiles of the set* (54) *in the case of the fractional Brownian motion* $(d = 1)$ *to the quantiles of the cumulative distribution function of a* $\mathcal{N}(0, 1)$ *Gaussian random variable.*

is a continuous function on $\mathbb{R}$. Moreover, since

$$\lim_{x\to-\infty}\left\{\begin{matrix}\widehat{F}_{H,J}^{(d)}\\ F_H^{(d)}\end{matrix}\right\}(x)=0 \quad \text{and} \quad \lim_{x\to+\infty}\left\{\begin{matrix}\widehat{F}_{H,J}^{(d)}\\ F_H^{(d)}\end{matrix}\right\}(x)=1,$$

the conclusion follows from Dini's theorem applied on the compact $\mathbb{R}\cup\{\pm\infty\}$ to the sequence of almost surely nondecreasing functions $(\widehat{F}_{H,J}^{(d)})_{J\in\mathbb{N}}$ which, according to (53), almost surely simply converges to the continuous function $F_H^{(d)}$. □

Based on our simulation procedure, we approximate $\widehat{F}_{H,J}^{(d)}(x)$ by

$$\frac{1}{\#\mathcal{D}_J}\sum_{m\in\mathcal{D}_J}\mathbb{1}_{\{2^{JH}(s_{m,J}-s_{m-1,J})\le x\}}$$

and we test the Gaussianity of the process by comparing this function to the cumulative distribution function Φ of a $\mathcal{N}(0, 1)$ Gaussian random variable. Figures 9 to 11 present the

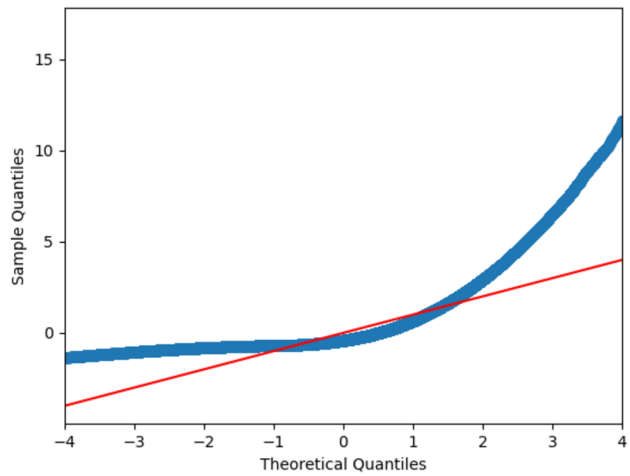

FIG. 10. *Qq-plot comparing the empirical quantiles of the set* (54) *in the case of the Rosenblatt process* $(d = 2)$ *to the quantiles of the cumulative distribution function of a* $\mathcal{N}(0, 1)$ *Gaussian random variable.*

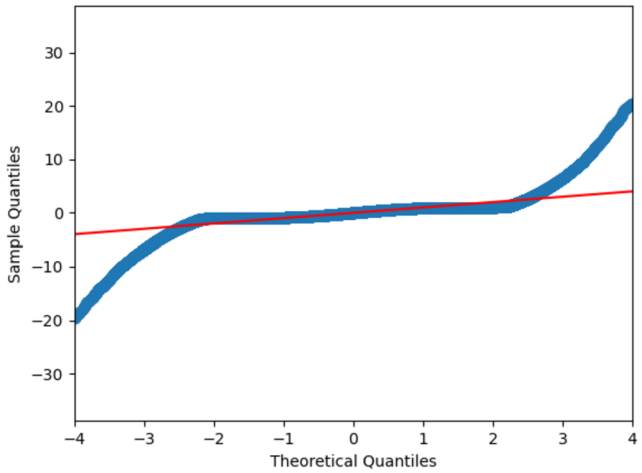

FIG. 11. *Qq-plot comparing the empirical quantiles of the set* (54) *in the case of the Hermite process of order* 3 ($d = 3$) *to the quantiles of the cumulative distribution function of a* $\mathcal{N}(0, 1)$ *Gaussian random variable.*

qq-plot obtained by comparing the empirical quantiles of the set

$$\left\{2^{JH}(s_{m,J} - s_{m-1,J})\right\}_{m\in\mathcal{D}_J} \tag{54}$$

to the quantiles of Φ. They clearly show that the latter set is normally distributed when $d = 1$, while it is not the case when $d = 2$ or $d = 3$. Interestingly, we also note that this approach seems to distinguish the Rosenblatt process from the Hermite process of order 3. This feature could be explored to develop a statistical method allowing to determne the order of a given Hermite process.

5.2. *Roles of the parameters.* The trajectories we simulate depend on the parameters $J \in \mathbb{N}$, $\varepsilon > 0$ and $a \in (1/2, 1)$. Undeniably, the most important parameter is J, since it alone truly governs the quality of the approximation provided by Theorems 2.12 and 2.13 as well as the size (41) of the data set (40) we simulate. According to (41), for any $T > 0$, $\#\mathcal{I}_J(T) \approx 2^J T$, thus it is clear that the complexity algorithm is exponential in J. Experimentally, we manage to produce a few simulations within a reasonable time up to the rather high level $J = 20$. However, if we wish to generate numerous simulations for statistical estimations, as we did above, we lower this threshold to $J = 17$. Nevertheless, Tables 5 and 6 below show that the Hurst parameter estimations are already quite satisfactory, especially for the QV estimator, at the reduced level $J = 12$.

The parameters a and ε do not play an explicit role in the convergence rate stated in Theorems 2.12 and 2.13. Nevertheless, the proofs of the latter two theorems as well as that of

TABLE 5
LW estimations of the Hurst parameter for simulations at resolution $J = 12$

		0.6	0.7	0.8	0.9
FBM	m	0.59	0.693	0.796	0.896
	s	0.016	0.016	0.016	0.019
RP	m	0.625	0.733	0.806	0.874
	s	0.032	0.035	0.034	0.042
HP	m	0.635	0.736	0.822	0.925
	s	0.040	0.030	0.032	0.038

TABLE 6
QV estimations of the Hurst parameter for simulations at resolution $J = 12$

		0.6	0.7	0.8	0.9
FBM	m	0.606	0.707	0.811	0.908
	s	0.017	0.017	0.021	0.018
RP	m	0.586	0.696	0.797	0.880
	s	0.037	0.029	0.027	0.022
HP	m	0.592	0.700	0.795	0.894
	s	0.045	0.033	0.021	0.010

Theorem 2.7 (see the proofs of Lemmata 3.1, 3.2, 3.3 and 3.6), which provide the theoretical validation of our method, explicitly depend on these parameters.

The parameter a determines the first and last time at which the process is simulated, see Remark 3.7. One may think that it could affect the quality of the approximation given by $\{S^{(d)}_{\mathbf{h},J}\}_{t\in\mathbb{R}_+}$ or $\{\widetilde{S}^{(d)}_{\mathbf{h},J}\}_{t\in\mathbb{R}_+}$. Indeed, the trajectory of this process is set to zero on $[0, m_0 2^{-J}]$. Thus, for instance, variations on $[0, m_0 2^{-J}]$ are vanishing, which could be a bad feature for estimators based on variations over an interval $[0, T]$. However, comparing Table 7 ($a = 0.51$) with Tables 3 ($a = 0.99$), we see that the value of a does not have a significant impact on the estimations of H. As the value of a does not affect the computational cost of the algorithm, we do not see any "advantageous" value to choose in practice. Maybe, taking a close to 1 is better to reduce edge effects in other applications.

The parameter $\varepsilon > 0$ has a real impact on the computational cost of the algorithm. Indeed, for any $t > 0$, $\#\mathcal{J}_J(t) \approx 2^{J(1+\varepsilon(d-1))}$. One might expect that working with larger values of ε improves the quality of the approximation, as it effectively adds more detail to the sums in (25). However, this is difficult to assess numerically. For instance, $\varepsilon = 1$ leads to considerable computation times as early as $d = 2$, making it impossible to generate a sufficiently large sample within a reasonable time frame. With $J = 17$ and $\varepsilon = 10^{-1}$, we have

$$\mathcal{J}^1_J(t) := \Big\{\mathbf{k} \in \big(D^1_J(t)\big)^d : \max_{\ell,\ell'\in[\![1,d]\!]} |k_\ell - k_{\ell'}| \le 3\Big\}$$

whereas for any $n \ge 2$ and $\varepsilon = 10^{-n}$,

$$\mathcal{J}^1_J(t) := \Big\{\mathbf{k} \in \big(D^1_J(t)\big)^d : \max_{\ell,\ell'\in[\![1,d]\!]} |k_\ell - k_{\ell'}| \le 1\Big\}.$$

We then simply compare the results above with estimates obtained from simulations using $\varepsilon = 10^{-1}$. Comparing Tables 8 and 9 with Tables 1 and 3 show that there is no real advantage in working with $\varepsilon = 10^{-1}$: the computation time is higher, for simulations of similar

TABLE 7
QV estimations of the Hurst parameter for simulation with $a = 0.51$

		0.6	0.7	0.8	0.9
FBM	m	0.606	0.707	0.807	0.905
	s	0.006	0.005	0.005	0.006
RP	m	0.587	0.691	0.799	0.897
	s	0.012	0.014	0.014	0.011
HP	m	0.588	0.691	0.796	0.897
	s	0.026	0.023	0.019	0.007

TABLE 8
LW estimations of the Hurst parameter for simulations with $\varepsilon = 10^{-1}$

		0.6	0.7	0.8	0.9
FBM	m	0.600	0.699	0.798	0.898
	s	0.004	0.004	0.003	0.003
RP	m	0.656	0.724	0.801	0.878
	s	0.008	0.011	0.013	0.013
HP	m	0.658	0.716	0.793	0.901
	s	0.016	0.016	0.014	0.016

TABLE 9
QV estimations of the Hurst parameter for simulations with $\varepsilon = 10^{-1}$

		0.6	0.7	0.8	0.9
FBM	m	0.606	0.711	0.813	0.919
	s	0.018	0.021	0.021	0.016
RP	m	0.557	0.687	0.804	0.909
	s	0.033	0.030	0.028	0.021
HP	m	0.556	0.685	0.805	0.900
	s	0.042	0.037	0.020	0.012

TABLE 10
LW estimations of the Hurst parameter with Vladas Pipiras's synthesis

		0.6	0.7	0.8	0.9
RP1	m	0.632	0.709	0.796	0.885
	s	0.009	0.015	0.021	0.025
RP2	m	0.617	0.711	0.800	0.891
	s	0.025	0.014	0.021	0.023

TABLE 11
LV estimations of the Hurst parameter with Vladas Pipiras's synthesis

		0.6	0.7	0.8	0.9
RP1	m	0.616	0.689	0.772	0.861
	s	0.021	0.027	0.037	0.043
RP2	m	0.615	0.694	0.781	0.869
	s	0.049	0.029	0.037	0.036

TABLE 12
QV estimations of the Hurst parameter with Vladas Pipiras's synthesis

		0.6	0.7	0.8	0.9
RP1	m	0.607	0.710	0.809	0.903
	s	0.026	0.024	0.022	0.019
RP2	m	0.610	0.705	0.809	0.905
	s	0.023	0.025	0.020	0.024

performance. If technological improvements in the near future make it possible to consider simulations at much higher resolutions J, it would be interesting to reassess the actual impact of ε. In particular, can ε be chosen as a function of J to obtain more refined simulations with reduced computational time? It is also possible that our theoretical results could be improved to eliminate the dependence on the parameter ε. Section 5 of Paper [38] seems to suggest that this is possible for the Rosenblatt process. Further investigation is, however, necessary in the case of a general Hermite process.

To obtain the results in Section 3 ensuring the theoretical validity of our approach, we explicitly needed to exploit the parameters $a \in (1/2, 1)$ and $\varepsilon > 0$ to bound certain parts of the random series (15) and (16). However, it is true that the exact values of $a \in (1/2, 1)$ and $\varepsilon > 0$ ultimately do not contribute to the rate of convergence in Theorems 2.12 and 2.13 and do not seem to affect the practical quality of the simulations either. It is therefore conceivable that our approach for proving some intermediate results is not yet fully optimal, and that we could eventually allow ourselves to take, for example, $\varepsilon = 0$ and $a = 1$. Nevertheless, we have not managed to dispense with these parameters and therefore still prefer to use them in our procedure to guarantee its theoretical validity. Future investigations may allow us to further improve our results.

5.3. *Comparisons with other methods.* Vladas Pipiras kindly shared with us his two wavelet-based synthesis of the Rosenblatt process [1, 38]. Tables 10 to 12 presented some Hurst parameter estimations of trajectories with prescribed Hurst parameter 0.6, 0.7, 0.8 and 0.9 realised with Vladas Pipiras's first synthesis method (RP1) and second synthesis method (RP2). In each cases, we simulated 100 trajectories on $[0, 1]$ with resolution $J = 17$ (which means that data are simulated at time $t = \frac{k}{2^J}$ with $0 \leq k \leq 2^J$). It shows that the three methods have similar performance in terms of Hurst index estimation, with perhaps a slight advantage for our approach. Nevertheless, we emphasize that Vladas Pipiras's methods require the numerical computation of fewer quantities (his approach is comparable to taking $\varepsilon = 0$ in ours) and therefore has a significantly lower computational cost.

In the case of fractional Brownian motion, since exact simulation methods are available, they are certainly more suitable in practice. On the other hand, we emphasize once again that our approach is unique for Hermite processes of order strictly greater than 2.

Acknowledgements. The authors are very grateful to the two anonymous referees for their valuable comments which have led to improvements of the article. Also they are very grateful to Vladas Pipiras who kindly shared with them his two wavelet-based synthesis of the Rosenblatt process.

Funding. Antoine Ayache acknowledges partial support from the Australian Research Council's Discovery Projects funding scheme (project number DP220101680). Also, he has been partially supported by the CDP C2EMPI, as well as the French State under the France-2030 programme, the University of Lille, the Initiative of Excellence of the University of Lille, the European Metropolis of Lille by their funding and support of the R-CDP-24-004-C2EMPI project.

Laurent Loosveldt acknowledges support from the FRNS Research Credit grant J.0136.26 "NOISE".

REFERENCES

[1] ABRY, P. and PIPIRAS, V. (2006). Wavelet-based synthesis of the Rosenblatt process. *Signal Process.* **86** 2326–2339. Special Section: Signal Processing in UWB Communications. https://doi.org/10.1016/j.sigpro.2005.10.021

[2] ABRY, P. and SELLAN, F. (1996). The wavelet-based synthesis for fractional Brownian motion proposed by F. Sellan and Y. Meyer: Remarks and fast implementation. *Appl. Comput. Harmon. Anal.* **3** 377–383. MR1420505 https://doi.org/10.1006/acha.1996.0030

[3] ASSAAD, O. and TUDOR, C. A. (2020). Parameter identification for the Hermite Ornstein–Uhlenbeck process. *Stat. Inference Stoch. Process.* **23** 251–270. MR4123924 https://doi.org/10.1007/s11203-020-09219-z

[4] AYACHE, A. and ESMILI, Y. (2020). Wavelet-type expansion of the generalized Rosenblatt process and its rate of convergence. *J. Fourier Anal. Appl.* **26** Paper No. 51, 35. MR4110623 https://doi.org/10.1007/s00041-020-09757-3

[5] AYACHE, A., HAMONIER, J. and LOOSVELDT, L. (2025). Wavelet-type expansion of generalized Hermite processes with rate of convergence. *Constr. Approx.* **61** 535–601. MR4922853 https://doi.org/10.1007/s00365-024-09692-2

[6] AYACHE, A. and TUDOR, C. A. (2024). Asymptotic normality for a modified quadratic variation of the Hermite process. *Bernoulli* **30** 1154–1176. MR4699548 https://doi.org/10.3150/23-bej1627

[7] BAI, S. and TAQQU, M. S. (2014). Generalized Hermite processes, discrete chaos and limit theorems. *Stoch. Process. Appl.* **124** 1710–1739. MR3163219 https://doi.org/10.1016/j.spa.2013.12.011

[8] BARDET, J.-M. and TUDOR, C. (2014). Asymptotic behavior of the Whittle estimator for the increments of a Rosenblatt process. *J. Multivariate Anal.* **131** 1–16. MR3252632 https://doi.org/10.1016/j.jmva.2014.06.012

[9] BARDET, J.-M. and TUDOR, C. A. (2010). A wavelet analysis of the Rosenblatt process: Chaos expansion and estimation of the self-similarity parameter. *Stoch. Process. Appl.* **120** 2331–2362. MR2728168 https://doi.org/10.1016/j.spa.2010.08.003

[10] BERAN, J. (2017). *Statistics for Long-Memory Processes*. Routledge, London. https://doi.org/10.1201/9780203738481

[11] CHRONOPOULOU, A., TUDOR, C. A. and VIENS, F. G. (2011). Self-similarity parameter estimation and reproduction property for non-Gaussian Hermite processes. *Commun. Stoch. Anal.* **5** 161–185. MR2808541 https://doi.org/10.31390/cosa.5.1.10

[12] CHRONOPOULOU, A. and VIENS, F. G. (2010). Hurst index estimation for self-similar processes with long-memory. In *Recent Development in Stochastic Dynamics and Stochastic Analysis. Interdiscip. Math. Sci.* **8** 91–117. World Scientific, Hackensack, NJ. MR2807815 https://doi.org/10.1142/9789814277266_0006

[13] CLAUSEL, M., ROUEFF, F., TAQQU, M. S. and TUDOR, C. (2014). Wavelet estimation of the long memory parameter for Hermite polynomial of Gaussian processes. *ESAIM Probab. Stat.* **18** 42–76. MR3143733 https://doi.org/10.1051/ps/2012026

[14] COEURJOLLY, J.-F. and PORCU, E. (2018). Fast and exact simulation of complex-valued stationary Gaussian processes through embedding circulant matrix. *J. Comput. Graph. Statist.* **27** 278–290. MR3816264 https://doi.org/10.1080/10618600.2017.1385468

[15] COEURJOLLY, J. F. (2000). Simulation and identification of the fractional Brownian motion: A bibliographical and comparative study. *J. Stat. Softw.* **5** 1–53. https://doi.org/10.18637/jss.v005.i07

[16] CRAIGMILE, P. F. (2003). Simulating a class of stationary Gaussian processes using the Davies–Harte algorithm, with application to long memory processes. *J. Time Series Anal.* **24** 505–511. MR2011811 https://doi.org/10.1111/1467-9892.00318

[17] DAHLHAUS, R. (1989). Efficient parameter estimation for self-similar processes. *Ann. Statist.* **17** 1749–1766. MR1026311 https://doi.org/10.1214/aos/1176347393

[18] DAVIES, R. B. and HARTE, D. S. (1987). Tests for Hurst effect. *Biometrika* **74** 95–101. MR0885922 https://doi.org/10.1093/biomet/74.1.95

[19] DIETRICH, C. R. and NEWSAM, G. N. (1997). Fast and exact simulation of stationary Gaussian processes through circulant embedding of the covariance matrix. *SIAM J. Sci. Comput.* **18** 1088–1107. MR1453559 https://doi.org/10.1137/S1064827592240555

[20] DOUKHAN, P., OPPENHEIM, G. and TAQQU, M. S., eds. (2003). *Theory and Applications of Long-Range Dependence* Birkhäuser, Boston, MA. MR1956041

[21] ECKSTEIN, E. C. (1991). Fractional Brownian motion and particle motions in blood flow. In *Proceedings of the Annual. International Conference of the IEEE Engineering in Medicine and Biology Society* **13**. IEEE Press, New York. https://doi.org/10.1109/iembs.1991.684981

[22] EMBRECHTS, P. and MAEJIMA, M. (2002). *Selfsimilar Processes. Princeton Series in Applied Mathematics*. Princeton Univ. Press, Princeton, NJ. MR1920153

[23] ESMILI, Y. (2020). Analyse par ondelettes de processus dans des chaos de Wiener. PhD thesis, Univ. Lille.

[24] FAUTH, A. and TUDOR, C. A. (2016). Multifractal random walk driven by a Hermite process. In *Handbook of High-Frequency Trading and Modeling in Finance. Wiley Handb. Finance Eng. Econom.* 221–249. Wiley, Hoboken, NJ. MR3585719

[25] FRANZKE, C. L. E., BARBOSA, S., BLENDER, R., FREDRIKSEN, H. B., LAEPPLE, T., LAMBERT, F., NILSEN, T., RYPDAL, K., RYPDAL, M. et al. (2020). The structure of climate variability across scales. *Rev. Geophys*. **58**. https://doi.org/10.1029/2019rg000657

[26] GIRAITIS, L. and TAQQU, M. S. (1999). Whittle estimator for finite-variance non-Gaussian time series with long memory. *Ann. Statist*. **27** 178–203. MR1701107 https://doi.org/10.1214/aos/1018031107

[27] HELGASON, H., PIPIRAS, V. S. and ABRY, P. (2011). Fast and exact synthesis of stationary multivariate Gaussian time series using circulant embedding. *Signal Process*. **91** 1123–1133. https://doi.org/10.1016/j.sigpro.2010.10.014

[28] LOOSVELDT, L. and TUDOR, C. A. (2025). Modified wavelet variation for the Hermite processes. *Electron. J. Stat*. **19** 2411–2455. MR4904494 https://doi.org/10.1214/25-ejs2390

[29] MANDELBROT, B. B. and VAN NESS, J. W. (1968). Fractional Brownian motions, fractional noises and applications. *SIAM Rev.* **10** 422–437. MR0242239 https://doi.org/10.1137/1010093

[30] MCGARRY, G. and DERICHE, M. Modelling mammographic images using fractional Brownian motion. In *TENCON '97 Brisbane—Australia. Proceedings of IEEE TENCON '97. IEEE Region* 10 *Annual Conference. Speech and Image Technologies for Computing and Telecommunications*. (*Cat. No.* 97*CH*36162). *TENCON*-97 **1** 299–302. IEEE Press, New York. https://doi.org/10.1109/tencon.1997.647316

[31] METZLER, R., JEON, J. H., CHERSTVY, A. G. and BARKAI, E. (2014). Anomalous diffusion models and their properties: Non-stationarity, non-ergodicity, and ageing at the centenary of single particle tracking. *Phys. Chem. Chem. Phys*. **16** 24128–24164. https://doi.org/10.1039/c4cp03465a

[32] MEYER, Y., SELLAN, F. and TAQQU, M. S. (1999). Wavelets, generalized white noise and fractional integration: The synthesis of fractional Brownian motion. *J. Fourier Anal. Appl*. **5** 465–494. MR1755100 https://doi.org/10.1007/BF01261639

[33] MORAN, P. A. and WHITTLE, P. (1951). Hypothesis testing in time series analysis. *J. R. Stat. Soc. A, General* **114** 579. https://doi.org/10.2307/2981095

[34] MOULINES, E. and SOULIER, P. (2003). Semiparametric spectral estimation for fractional processes. In *Theory and Applications of Long-Range Dependence* 251–301. Birkhäuser, Boston, MA. MR1956053

[35] NORROS, I. (1995). On the use of fractional Brownian motion in the theory of connectionless networks. *IEEE J. Sel. Areas Commun*. **13** 953–962. https://doi.org/10.1109/49.400651

[36] NOURDIN, I. and PECCATI, G. (2012). *Normal Approximations with Malliavin Calculus*: *From Stein's Method to Universality*. *Cambridge Tracts in Mathematics* **192**. Cambridge Univ. Press, Cambridge. MR2962301 https://doi.org/10.1017/CBO9781139084659

[37] PAN, J. (2007). Fractional Brownian motion and the halo mass function. *Mon. Not. R. Astron. Soc. Lett*. **374** L6–L9. https://doi.org/10.1111/j.1745-3933.2006.00253.x

[38] PIPIRAS, V. (2004). Wavelet-type expansion of the Rosenblatt process. *J. Fourier Anal. Appl*. **10** 599–634. MR2105535 https://doi.org/10.1007/s00041-004-3004-y

[39] PIPIRAS, V. (2005). Wavelet-based simulation of fractional Brownian motion revisited. *Appl. Comput. Harmon. Anal*. **19** 49–60. MR2147061 https://doi.org/10.1016/j.acha.2005.01.002

[40] PIPIRAS, V. and TAQQU, M. S. (2017). *Long-Range Dependence and Self-Similarity*. *Cambridge Series in Statistical and Probabilistic Mathematics* **45**. Cambridge Univ. Press, Cambridge. MR3729426

[41] RASMUSSEN, C. E. and WILLIAMS, C. K. I. (2006). *Gaussian Processes for Machine Learning*. *Adaptive Computation and Machine Learning*. MIT Press, Cambridge, MA. MR2514435

[42] ROBINSON, P. M. (1995). Gaussian semiparametric estimation of long range dependence. *Ann. Statist*. **23** 1630–1661. MR1370301 https://doi.org/10.1214/aos/1176324317

[43] SAMKO, S. G., KILBAS, A. A. and MARICHEV, O. I. (1993). *Fractional Integrals and Derivatives*: *Theory and Applications*. Gordon & Breach, Yverdon. Edited and with a foreword by S. M. Nikol'skiĭ. Translated from the 1987 Russian original. Revised by the authors. MR1347689

[44] SAMORODNITSKY, G. (2016). *Stochastic Processes and Long Range Dependence*. *Springer Series in Operations Research and Financial Engineering*. Springer, Cham. MR3561100 https://doi.org/10.1007/978-3-319-45575-4

[45] SCHWARTZ, L. (1978). *Théorie des Distributions*. Hermann, Paris. MR0209834

[46] SHIGEKAWA, I. (1980). Derivatives of Wiener functionals and absolute continuity of induced measures. *J. Math. Kyoto Univ*. **20** 263–289. MR0582167 https://doi.org/10.1215/kjm/1250522278

[47] STOYANOV, S. V., RACHEV, S. T., MITTNIK, S. and FABOZZI, F. J. (2019). Pricing derivatives in Hermite markets. *Int. J. Theor. Appl. Finance* **22** 1950031, 27. MR4028644 https://doi.org/10.1142/s0219024919500316

[48] TAQQU, M. S. (1978). A representation for self-similar processes. *Stoch. Process. Appl*. **7** 55–64. MR0492691 https://doi.org/10.1016/0304-4149(78)90037-6

[49] TORRES, S. and TUDOR, C. A. (2009). Donsker type theorem for the Rosenblatt process and a binary market model. *Stoch. Anal. Appl*. **27** 555–573. MR2523182 https://doi.org/10.1080/07362990902844371

[50] TUDOR, C. (2023). *Non-Gaussian Selfsimilar Stochastic Processes*. *SpringerBriefs in Probability and Mathematical Statistics*. Springer, Cham. MR4647498 https://doi.org/10.1007/978-3-031-33772-7

[51] TUDOR, C. A. and VIENS, F. G. (2009). Variations and estimators for self-similarity parameters via Malliavin calculus. *Ann. Probab.* **37** 2093–2134. MR2573552 https://doi.org/10.1214/09-AOP459

[52] VIVEK, K. S. and CHAURASIA, A. (2019). Synthetic traffic generation for wavelet based Rosenblatt process using LSTM for multicore architecture. *Int. J. Control Autom.* **12** 607–617.

[53] WHITTLE, P. (1962). Gaussian estimation in stationary time series. *Bull. Inst. Int. Stat.* **39** 105–129. MR0162345

[54] WOOD, A. T. A. and CHAN, G. (1994). Simulation of stationary Gaussian processes in $[0, 1]^d$. *J. Comput. Graph. Statist.* **3** 409–432. MR1323050 https://doi.org/10.2307/1390903